

AD-A106 154

NAVAL RESEARCH LAB WASHINGTON DC
COMPUTATIONAL STUDY OF MAGNETIC DAM EFFECTS IN A HIGH IMPEDANCE--ETC(U)
OCT 81 R J BARKER, S A GOLDSTEIN, A T DROBOT

F/G 20/7

UNCLASSIFIED

NRL-MR-4642

NJ

1 OF 1
AD A
106154

END
DATE
FILMED
11-81
DTIC

LEVEL II

2

NRL Memorandum Report 4642

**Computational Study of Magnetic Dam Effects
in a High Impedance Diode**

R. J. BARKER AND SHYKE A. GOLDSTEIN

*JAYCOR, Inc.
Alexandria, VA 22304*

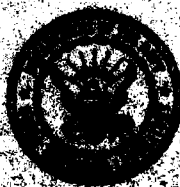
A. T. DROBOT

*Science Applications, Inc.
McLean, VA 22102*

**DTIC
ELECTE
S OCT 26 1981 D
E**

October 14, 1981

**This research was sponsored in part by the Defense Nuclear Agency under
Contract F49620-81-1-014, work unit 46, and work unit title "Ion Beam
Generation," and by the Department of Energy, Washington, DC.**



DEFENSE NUCLEAR AGENCY

Approved for public release; distribution unlimited

81 10 14

FILE COPY

9) REPORT DOCUMENTATION PAGE		READ INSTRUCTIONS BEFORE COMPLETING FORM
1. REPORT NUMBER NRL Memorandum Report 4642	2. GOVT ACCESSION NO.	3. RECIPIENT'S CATALOG NUMBER
6. TITLE (and Subtitle) COMPUTATIONAL STUDY OF MAGNETIC DAM EFFECTS IN A HIGH IMPEDANCE DIODE.	5. TYPE OF REPORT & PERIOD COVERED Interim report on a continuing NRL problem.	
	6. PERFORMING ORG. REPORT NUMBER	
7. AUTHOR(s) R.J. Barker, Shyke A. Goldstein, A.T. Drobot	8. CONTRACT OR GRANT NUMBER(s) 11) 24 Oct 81	
9. PERFORMING ORGANIZATION NAME AND ADDRESS Naval Research Laboratory Washington, DC 20375	10. PROGRAM ELEMENT, PROJECT, TASK AREA & WORK UNIT NUMBERS 47-0875-01; ES-77-A-01-6021; 47-0879-01	
11. CONTROLLING OFFICE NAME AND ADDRESS Department of Energy Defense Nuclear Agency Washington, DC 20545 Washington, DC 20305	12. REPORT DATE October 14, 1981	
	13. NUMBER OF PAGES 40 (12) 42	
14. MONITORING AGENCY NAME & ADDRESS (if different from Controlling Office) 14. NRL-MR-4642	15. SECURITY CLASS (of this report) UNCLASSIFIED	
	15a. DECLASSIFICATION DOWNGRADING SCHEDULE	
16. DISTRIBUTION STATEMENT (of this Report) Approved for public release; distribution unlimited.		
17. DISTRIBUTION STATEMENT (of the abstract entered in Block 20, if different from Report)		
18. SUPPLEMENTARY NOTES *Present address: Jaycor Inc., Alexandria, VA 22304 †Present address: Science Applications, Inc., McLean VA 22102 (Continues)		
19. KEY WORDS (Continue on reverse side if necessary and identify by block number) Numerical simulation Intense ion beams		
20. ABSTRACT (Continue on reverse side if necessary and identify by block number) Computer simulations have been conducted to test the "magnetic dam" concept as a means for boosting the overall ion efficiency of high impedance diodes. The "dam" consists of a cell located immediately behind the anode foil containing a wire along its central axis which carries a current flowing in a direction opposite to that in the diode gap. The azimuthal magnetic field generated by the wire current, I_w , reflects the electrons crossing the foil back into the A-K gap at higher radii where their space charge can enhance ion (Continues)		

232700

18. Supplementary Notes (Continued)

This research was sponsored in part by the Defense Nuclear Agency under Subtask T99QAXLA014, work unit 46 and work unit title "Ion Beam Generation" and by the Department of Energy, Washington, DC.

20. Abstract (Continued)

emission over relatively large areas. Significant increases in the ion current were observed for several values of I_w but a simultaneous increase in electron current prevented gains in overall ion efficiency. Instead, only decreased impedances were observed. The cause of this phenomenon is explained and indicates solutions which could benefit a wide range of future diode designs.

CONTENTS

I. INTRODUCTION 1

II. THEORY OF THE MAGNETIC "DAM" 3

III. THE NUMERICAL SIMULATION 6

IV. RESULTS 14

REFERENCES 30

Accession For		
NTIS GRA&I	<input checked="" type="checkbox"/>	
DTIC TAB	<input type="checkbox"/>	
Unannounced	<input type="checkbox"/>	
Justification		
By		
Dist. Statement		
Availability Codes		
Availability Statement/ or		
Dist. Statement		
A		

COMPUTATIONAL STUDY OF MAGNETIC DAM EFFECTS
IN A HIGH IMPEDANCE DIODE

I. INTRODUCTION

The NRL Light Ion Fusion Program has experimentally demonstrated high efficiencies for the production of light ion beams using low impedance diodes. On Gamble II in 1-2 ohm operation well over 70% of the diode power is typically carried by the ions.^{1,2} Current and planned experiments call for the design and use of diodes on the high impedance pulsed power generators of Harry Diamond Lab's AURORA and Sandia National Lab's PBFA II modules. Since impedance matching is essential for efficient transfer of power from the machine to the diode, these new diodes must be designed for 4-20 ohm operation. Unfortunately, it has been experimentally determined that efficiencies of only 20-50% can be obtained in this operating regime using traditional axial diode configurations.³ The development of techniques for boosting these relatively low ion production efficiencies is today the subject of intense research and speculation. This paper reports on the results of one such theoretical effort. Although the specific diode design which was simulated did not achieve the desired boost of ion efficiency, an examination of its shortcomings clearly indicates both a cause as well as possible solutions. These observations bear on high impedance axial diodes in general and lend a new insight into their peculiarities which may eventually assist in a design breakthrough.

Specifically, the diode geometry under consideration here would be suitable for operation on AURORA. It is drawn to scale in Figure 1 with all significant dimensions given, as indicated, in centimeters. Although the latest NRL/AURORA ion diode has an anode stalk almost 25 cm in radius, its cathode shank remains about 5 cm in radius. The differences caused by modifications to the electric field beyond $R = 7$ cm are assumed to be minor, since they do not directly effect electron motion in the active anode-cathode(A-K) gap. The diode modeled was chosen for positive polarity operation. That is, the resultant ion beam would be traveling through the cathode shank in a direction away from the generator and pulse-forming line. The inner and outer radii of the vacuum feed line are 8.0 and 10.0 centimeters, respectively. The anode is a simple hollow cylinder with a wall one-half centimeter thick which is capped by two 4 mil. polyethylene foils separated by a one-quarter centimeter vacuum gap. It is important that the electron beam traveling through the cell behind the anode foil be charged and current neutralized. It is widely believed that a gas fill at several torr pressure could provide the assumed neutralization. A thin wire is located along the anode's central axis and is electrically connected to it via the inner foil. Current of arbitrary magnitude may be fed through this wire from an external source which is independent of the pulsed power generator. Such a current of I_w amperes will create an azimuthal magnetic field behind the foil of

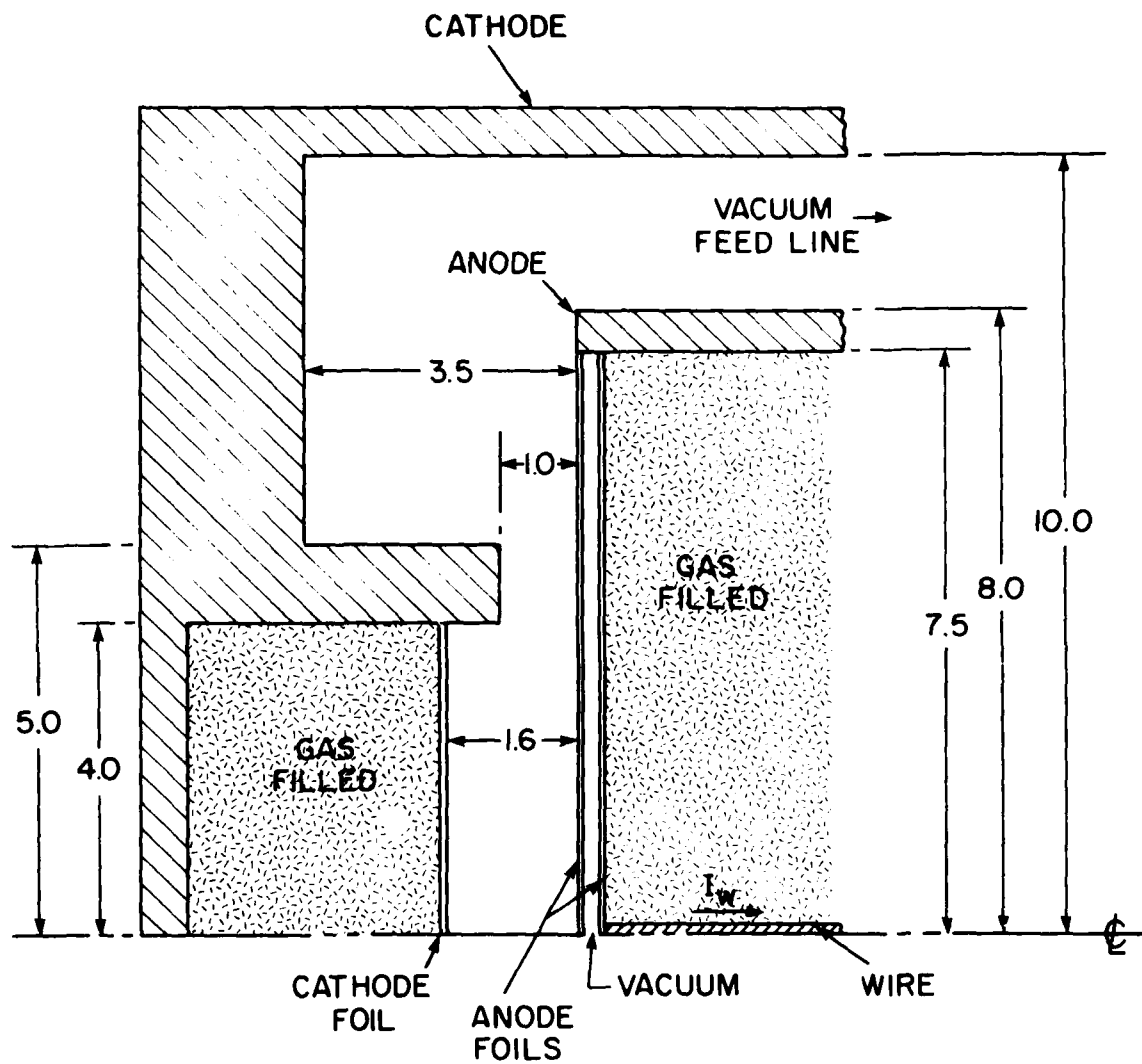


Fig. 1 - A scale drawing of the magnetic dam diode. (All dimensions are in centimeters.)

magnitude $\frac{0.2I_w}{r}$ gauss. If sufficiently strong, this B_θ can bend the

trajectories of electrons entering the anode gas cell near $r = 0$ in such a way as to "reflect" them out of the anode foil again at a higher radius. This effective barrier against axial electron flow is the essence of the magnetic dam concept. It is seen as a possible mechanism for increasing the average lifetime of a typical electron in the anode-cathode (A-K) gap. This should increase electron space charge for a given electron current, increasing the net ion emission.

In the given diode, the A-K gap was chosen to be one centimeter to allow approximately 6-8 ohm impedance at the fixed 4 megavolts applied. Finally, the hollow cathode has an outer radius of 5.0 cm. with 1.0 cm. shank thickness. A 4 mil polyethylene foil is recessed 0.6 cm into the shank to enclose a low-pressure gas fill similar to that of the anode and serving a similar charge/current neutralization role for the emerging ion beam. This cathode gas cell plays no part whatsoever in this simulation.

The analysis of this diode begins in Section II with a theoretical discussion of the "magnetic dam" principle. This will explain the motivation for conducting the simulation. Section III will transition into the actual numerics of the modeling, examining the details of the code that was employed. Specific approximations and assumptions used in the model will be pointed out. This report will conclude in the fourth section with a presentation of the simulation results complete with suggestions for follow-on work.

II. THEORY OF THE MAGNETIC "DAM"

The treatment of electron trajectories in an azimuthal magnetic field and in the absence of an electric field may be derived from an analysis of ion orbits due to Goldstein and Ottinger.⁴ The particle orbits may be determined from a simple conservation of energy principle. Consider an electron traveling at velocity, \vec{v} , impinging on the anode foil at some angle, θ , and entering the anode gas cell at radius, R_0 , as shown in Figure 2. In the gas cell, it is assumed to be acted upon only by the azimuthal magnetic field there. Its energy must therefore remain constant and

$$\gamma = \left(1 - \frac{v^2}{c^2}\right)^{-1/2} = \text{constant}, \quad (1)$$

where

$$v^2 = v_r^2 + v_z^2. \quad (2)$$

For an electron which has just crossed a cathode-anode gap with electric potential difference, V , in megavolts, it may be further written that

$$\gamma = 1 + \left| \frac{V}{0.511} \right|. \quad (3)$$

From Figure 2,

$$v_{z0} = v \sin\theta. \quad (4)$$

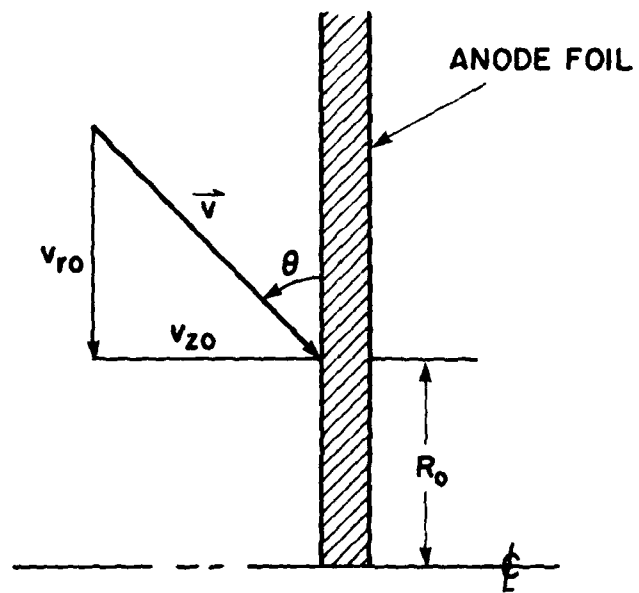


Fig. 2 — Geometry of electron penetration into the anode gas cell

Combining Eqs. (1), (3), and (4) yields

$$v_{z0} = c \sin \theta \sqrt{1 - \left(\frac{0.511}{v+0.511}\right)^2} \quad (5)$$

Furthermore, Eqs. (2) and (4) give a direct expression for the time dependence of the electron's radial velocity in the gas cell,

$$v_r(t) = \pm \sqrt{v_{z0}^2 \sin^{-2} \theta - v_z^2(t)} \quad (6)$$

The force acting upon the electron is given by the relativistic Lorentz Law to be

$$\gamma m_0 \frac{dv_z}{dt} = -\frac{e}{c} \vec{v}_r \times \vec{B}_\theta(r) = -\frac{e}{c} \frac{dr}{dt} B_\theta(r) \quad (7)$$

where m_0 is the electron rest mass. This equation may be rearranged and integrated from the foil entry point $(0, R_0, 0)$ out to some point along the electron's trajectory in the cell to yield

$$v_z(t) - v_{z0} = \frac{-e}{m_0 c \gamma} \int_{R_0}^r B_\theta(r) dr \quad (8)$$

As stated previously, the magnetic field in the gas cell generated by a current, I_w , flowing through the axial wire is simply $B_\theta(r) = 0.2 I_w/r$. Equation (8) may thus be rewritten as

$$v_z = v_{z0} \left(1 - \chi(r)\right) \quad (9)$$

where

$$\chi(r) \equiv \frac{0.2 e}{m_0 c v_{z0} \gamma} I_w \ln \frac{r}{R_0} \quad (10)$$

with I_w expressed in amperes and all other quantities in c.g.s. units. The orbit expression linking r explicitly to z is simply the ratio of the respective velocity components given in Eqs. (6) and (9),

$$\frac{dr}{dz} = \frac{v_r}{v_z} = \pm \frac{\sqrt{\sin^{-2} \theta - 1 + \chi(r)(2-\chi(r))}}{1 - \chi(r)} \quad (11)$$

The integration of Eq. (11) yields the exact trajectory of an electron traversing the gas-filled anode for specific values of θ , V , I_w , and R_0 .

It is instructive to calculate sample orbits for various combinations of parameters. In all cases, V is fixed at 4.0 megavolts in order to correspond to realistic AURORA ion diode operations. Useful choices for I_w can be estimated by a rather simple calculation. Consider a 4 MeV

electron with an entrance angle of 90° beginning its gas cell trajectory at a radius of 1.0 centimeter. Assume that it remains in a uniform azimuthal magnetic field of magnitude equal to that found at the exact center of its circular gyration in the actual gas cell. Therefore, for a desired exit radius of 5.0 centimeters, the value of $B_\theta(r)$ at $r = 3.0$ cm. is taken as a constant over the entire electron trajectory. In order to generate the field strength needed for a 2.0 centimeter relativistic gyroradius, a wire current of 63.75 kiloamps is required. This reasoning leads to the following selection of values for I_w to be tested: 65 kA, 130 kA, and 300 kA.

For the first set of sample orbits, an entrance angle of $\theta = 90^\circ$ is chosen. This choice leads to an orbit equation given by

$$\frac{dr}{dz} = \pm \sqrt{\frac{\chi(r)(2-\chi(r))}{1-\chi(r)}} \quad (12)$$

The trajectories for $R_0 = 1.0$ and $R_0 = 2.0$ cm. are plotted in Figure 3. It can be seen that $I_w = 65$ kA generates too weak a field to reflect electrons with R_0 greater than 1.0 cm. back into the A-K gap. The orbit for $R_0 = 1.0$ cm is marginal. On the other hand, $I_w = 130$ kA produces the desired effect for R_0 less than 2.0 cm and the $I_w = 300$ kA case is even better.

In a realistic pinch reflex diode configuration such as that being modeled, one expects to see a focused electron flow in which electrons magnetically self-pinch to smaller radii as they cross the gap. It is therefore important to attempt a similar orbit calculation for non-normally incident electrons. A reasonably straightforward, yet probably illustrative example would be electrons entering the gas cell at 45° . This choice of θ reduces Equation (11) to

$$\frac{dr}{dz} = \pm \sqrt{\frac{1+\chi(r)(2-\chi(r))}{1-\chi(r)}} \quad (13)$$

A new set of sample orbits is calculated and shown in Figure 4.

Comparison of the two sets of plots reveals immediately that non-perpendicular injection leads to electrons exiting the gas cell at significantly lower radii. This is reasonable considering the longer period of time a given electron spends in regions of relatively higher magnetic field strength. Their orbits consequently experience greater bending. The overall effect for all but the 65 kA cases is the satisfactory reflection of all electrons with $R_0 \leq 2.0$ cm back into the anode-cathode gap where they can enhance ion emission.

III. THE NUMERICAL SIMULATION

A. The Simulation Code

The computer code utilized in these studies is a 2-D version of the 2½-D DIODE2D⁵ particle-in-cell (P.I.C.) code. Inhomogeneities are allowed in the radial (r) and axial (z) spatial dimensions. Complete azimuthal symmetry is assumed. In addition, the r- and z- momentum components are retained. The "particles" in this model are axially-centered rings of charge. In reality they are macroparticles carrying many times an elementary charge

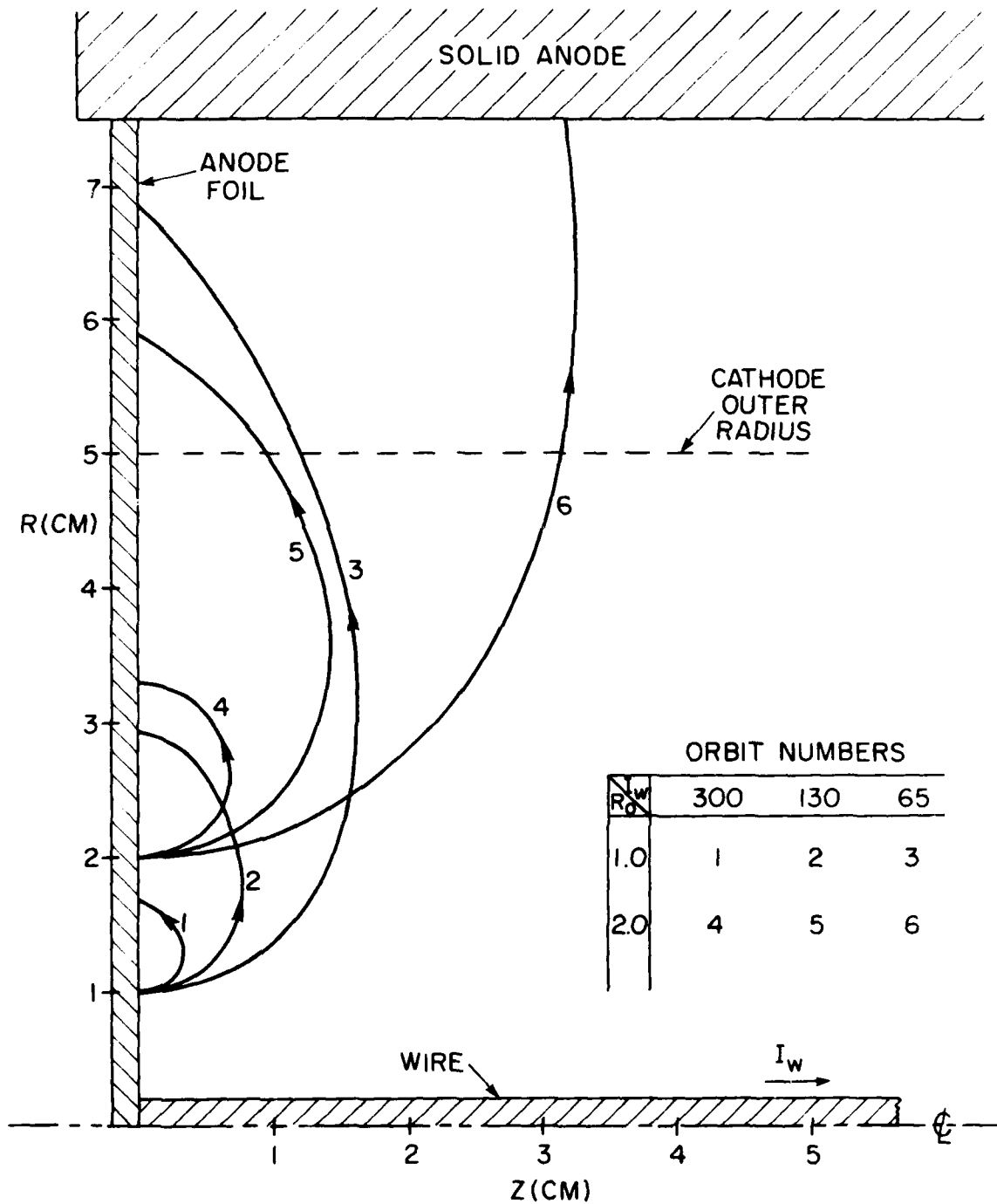


Fig. 3 - Sample 4 MeV electron orbits for 90° injection

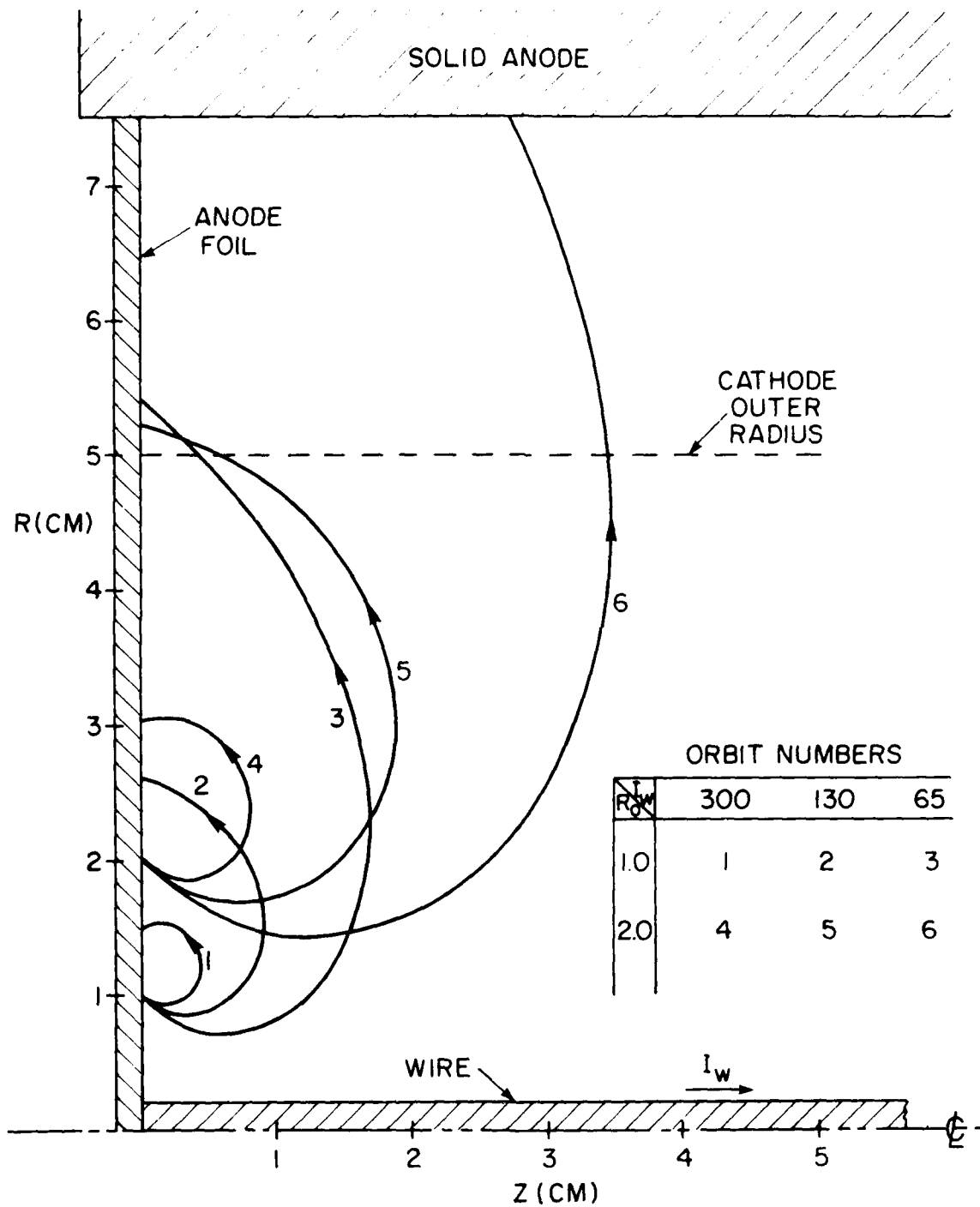


Fig. 4 - Sample 4 MeV electron orbits for 45° injection

but retaining the physical charge-to-mass ratios of the protons and electrons which they represent. Area weighting (i.e., linear interpolation) is used to couple these charges with the electric and magnetic fields calculated over a fixed set of grid-points in the region of interest. The fields thus interpolated to the particle positions act on these charge-current rings by way of the relativistic Lorentz force equation. The field treatment is electrostatic. In this sense the code does not perform a true "simulation" since the time-dependent equations are not observed. Rather the treatment is "quasistatic". Equilibrium solutions to various diode geometries are sought. The "timesteps" which appear in the code are actually snapshots of the system while it seeks to relax toward its steady-state configuration. In order to determine the electric field within the diode region, particle charge densities are distributed over a fixed grid and the discrete Poisson's equation is solved.⁶ The code permits irregular conducting boundaries inside the computational region. The treatment of such internal boundaries entails the use of a "capacitance matrix". The internal surfaces thus created are held at predetermined electric potential values. Direct radial integration of the axial current densities over the mesh yields the azimuthal magnetic field via Ampere's Law. The outer radial boundary of the diode region may be either conducting or free-space. The electrostatic potential, ϕ , is set constant along all conducting boundaries. Along radial free-space boundaries, ϕ is graded logarithmically and along axial ones, linearly.

At the start of a typical computer run, the computational diode region is a complete vacuum devoid of particles. The electric potential is pre-set along the entire boundary as well as along all internal conducting surfaces. The emission of the ions is permitted anywhere along fixed regions of the anode surface. Electrons are emitted along the entire cathode, including the inner and outer shank surfaces. The value of the perpendicular electric field at a given emission point determines the total charge (i.e., number of particles) that will be emitted there. At the beginning of a timestep, the electric field at a surface specifies the net charge density on the surface via Gauss' Law. The surface integral of this density over a cell width around a given grid point yields the net charge which is emitted there for that timestep. Prior to the actual particle-pushing the electric field is recalculated taking into account the newly emitted charge.

All particles are then pushed according to the relativistic Lorentz force law using the area weighted electric and magnetic field values interpolated at the particle position from the four nearest grid points. After pushing in each timestep a position check is performed on each particle to determine if it is inside a conductor or outside the mesh boundaries. If so, the particle is appropriately absorbed and so recorded. On the other hand if it is an electron in an anode foil, then it is passed to a scattering subroutine which employs a one-step Monte Carlo algorithm to calculate energy loss and deflection. Upon completion of this sorting process, the charge and current density associated with each unabsorbed particle is distributed over the four nearest grid points using the same linear interpolation scheme in reverse. This yields a complete array of values for the charge density, ρ , and the current density, J_z , over the computational mesh. Poisson solving these arrays yields ϕ from which E_r and E_z are calculated. The azimuthal component of \vec{B} is obtained through direct integration of J_z over the grid. Quantities of interest are then extracted and output via diagnostic

subroutines. The code then cycles to the next timestep for particle emission.

Finally, it should be noted that the numerics of the particle pushing as well as the potential solving has been completely "vectorized". Thus, the momentum, position, and field components associated with the entire ensemble of particles are treated as macro-vector quantities. Arithmetic operations performed with them are accomplished in a completely vector-array format. This property of the code permits efficient running times on the most advance scientific computers. (Of course, the interpolation of \vec{v} , \vec{J} , E , and B values between particle positions and grid points requires random accessing of array points and this process cannot be vectorized.)

B. The Computational Experiment

At the outset of this simulation, as with any other, great care was taken to minimize the numerical complexity/cost while preserving all aspects of the essential physics to be treated in the problem. It was this desire to minimize expense that motivated the use of a 2-D version of DIODE2D rather than its standard 2½-D form. (The standard version allows for solution of self B_r and B_z field components which are never generated here.) The second most significant economization involved the minimization of the physical size of the computational region. It was deemed uneconomical as well as physically unimportant to fill the entire diode cavity with the numerical grid. As can be seen from Figure 1, that would result in a mesh measuring about six centimeters axially by ten radially and would waste computational effort by including space devoid of particles. Instead, the axial extent of the grid was bounded by the plane of the cathode foil and by the inner anode foil. Similarly, its radial limit was set as the inner radius of the anode cylinder. The only obstacle to this reduction of grid extent was the free-space part of the new, artificial boundary. DIODE2D's field solving algorithm requires fixed potential values along all the boundaries. For the full diode with its conducting walls this is, of course, no problem. Even the open segment of the vacuum feed line entrance is trivial, since a simple logarithmic potential grading can be used there (assuming the presence of no particles there). The setting of potential values along the new, ad hoc boundaries cannot be accomplished intuitively. Instead, a two-step process is employed. First, a capacitance matrix field-solve is carried out for the entire diode cavity as pictured in Figure 5. It is assumed that no "sources" (i.e. charges or currents) are present anywhere. Then the new "boundaries" are located as indicated by the dotted lines, and the free-space potential values are noted. Finally the new computational region is set up with those values imposed along the appropriate edges. As long as no particles stray too "near" those ends, ϕ should remain fairly constant there. In any case, the bulk ion and electron flow should be too "remote" to feel any peripheral abnormalities. The vacuum potential solution for the actual simulation grid is shown in Figure 6. Note that the axial scaling is much finer than the radial in order to more fully appreciate the field profiles.

The final computational grid is depicted in Figure 7. It is spanned by 66 data cells in the axial dimension and 77 radially. Poisson-solving is accomplished on the interior 64 X 75 mesh, leaving a monolayer of "guard" cells along the boundary. Simple Gaussian field emission of electrons is permitted all along the heavy-lined surfaces of the cathode as shown in the

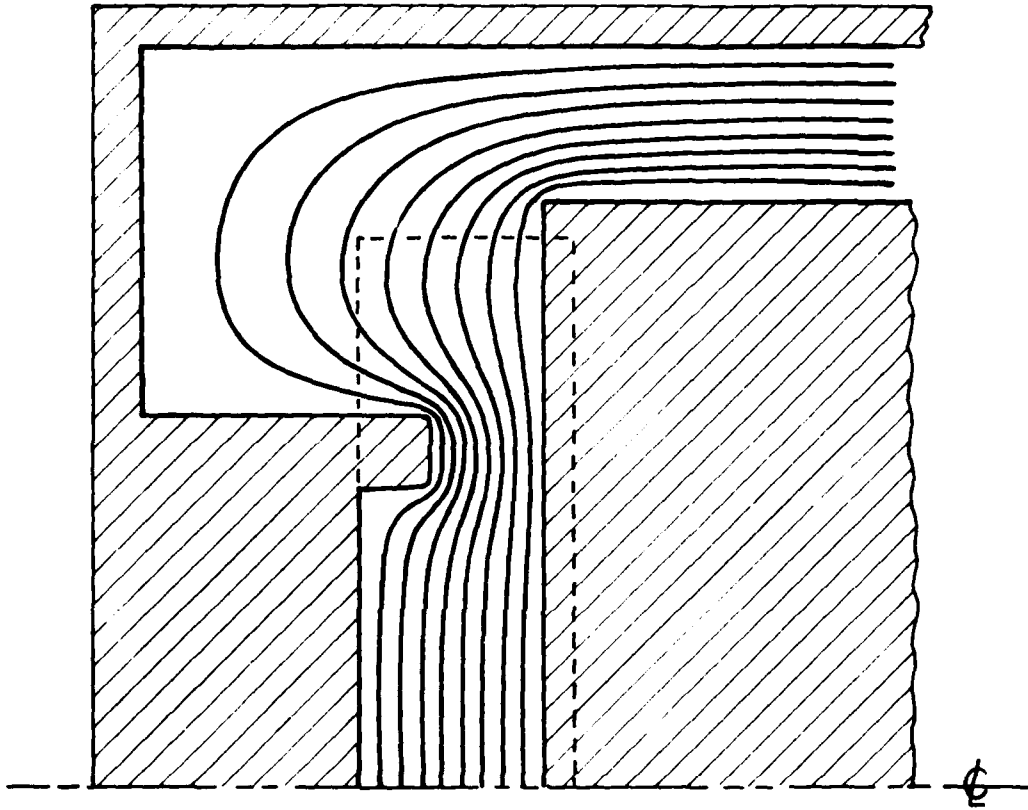


Fig. 5 — Vacuum equipotential plot for the entire diode

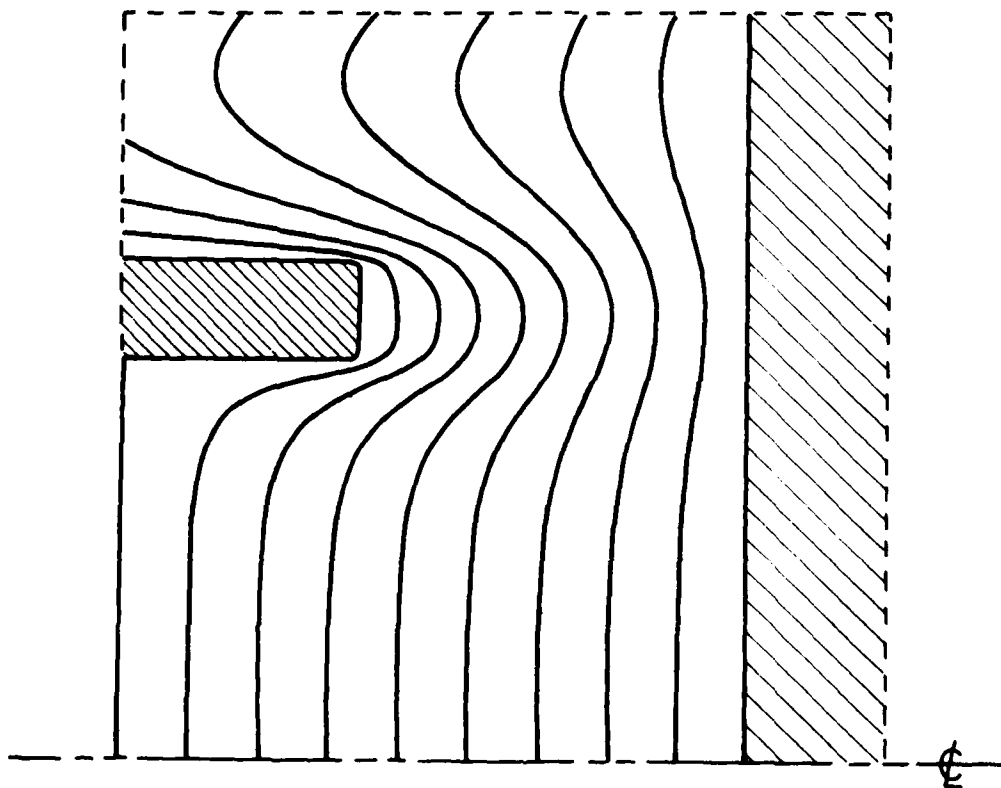


Fig. 6 - Vacuum equipotential plot for the restricted computational region

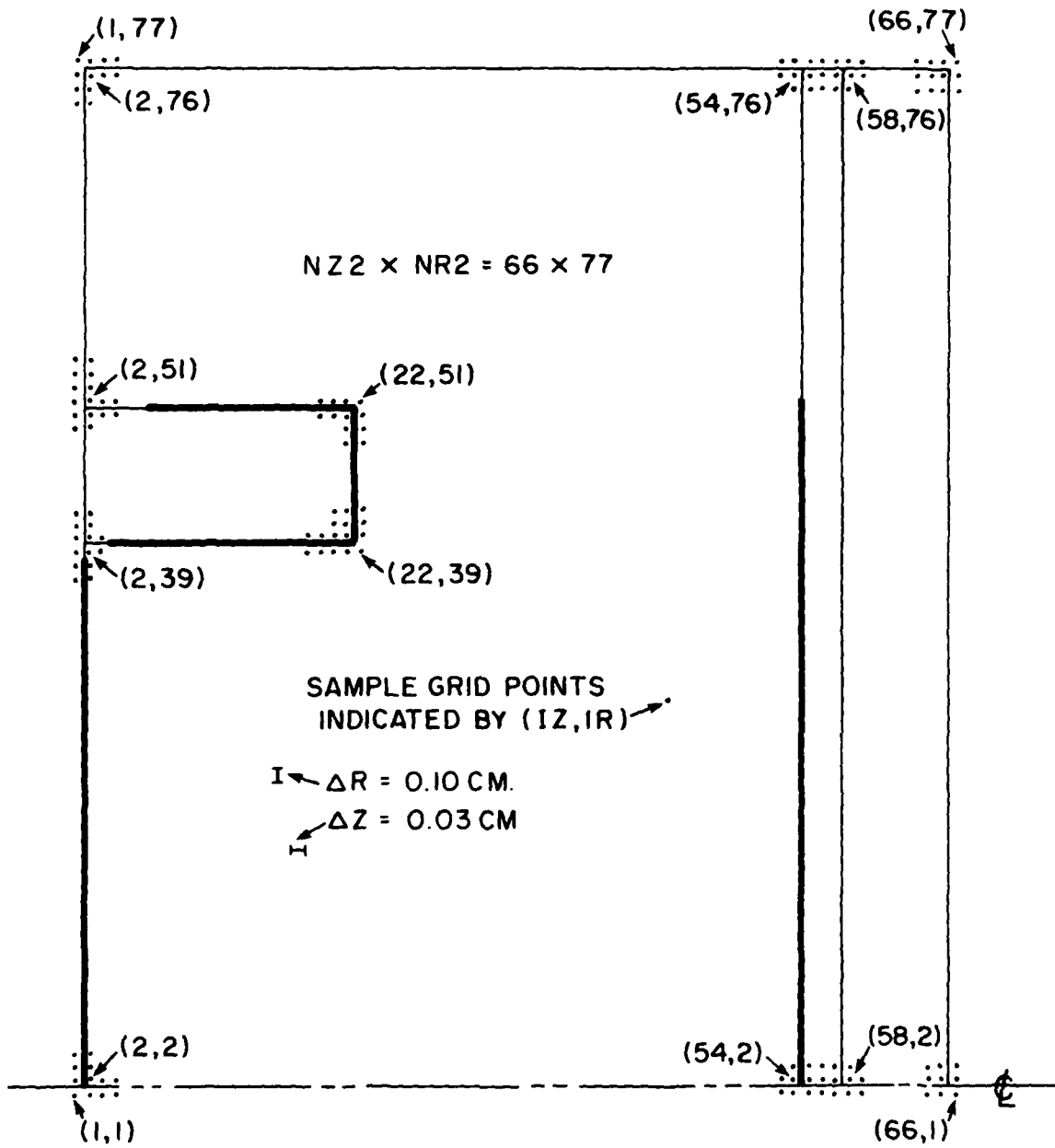


Fig. 7 - The numerical computation grid

figure. The same is true for ion emission along the outer surface of the anode foil. Note that no electron emission is allowed in either the region around point (2,39) of the inner cathode shank surface or along the rear of the outer shank. Electric field values are expected to be too imprecise there. The timestep was fixed at 1.5×10^{-12} second for most of the runs presented although smaller timesteps were used near steady state to test the stability of the equilibria. Another interesting point is the numerical "thickness" of the outer anode foil. Although physically treated as 4.0 mil thick polyethelene by DIODE2D's electron scattering algorithm, this foil spans three full cells spatially. This is an artifact to ensure that no electron will be able to traverse the foil in a single timestep. Since no fields act on particles inside the foil, this false thickness does not impact on the physics of the simulation itself. Among the most important of the code diagnostics are a complete record of time-averaged emission and absorption profiles for each of the surfaces, sample particle position plots, and electrostatic equipotential plots.

The numerical implementation of the physics of the magnetic dam involved non-trivial manipulation and reorganization of the standard DIODE2D algorithms. The region inside the gas cell, behind the inner anode foil was designed to be completely free of all electric and magnetic fields except for the azimuthal B-field due to the current-carrying wire along the axis. Therefore, no solutions of Poisson's equation nor radial integrations of Ampere's law were necessary there. Only $B_\theta = 0.2 I_w/r$ need be enforced. Thus, no extension of the field-solving and charge/current apportionment mesh was called for. Instead, the standard electron-absorbing character of the rightmost boundary was changed to complete transparency to electron flow. The particle accounting routines in the simulation were charged, such that an electron hitting that edge was not removed from the "active" particle list. Instead, it was given a special "label" which told the particle pushing subroutine to act on it only with a B_θ appropriate to its radial displacement, r , and to the I_w chosen for the wire current.

IV. RESULTS

In the initial simulation runs, the diode voltage was set at four megavolts and electron emission was turned on all along those cathode surfaces indicated in Figure 7. To limit the diode impedance, proton emission along the anode foil was not permitted beyond a radius of 5.0 centimeters. The early development of electron and ion flow patterns proceeded as illustrated in Figures 8a and 8b. In each plot of sample particle positions, note that the axial and radial dimension scales are not the same. Each frame measures 7.5 cm radially and just under two centimeters axially. The lower border of each frame is the diode centerline. In looking at these pictures, bear in mind that these are glimpses of a quasi-static simulation of particle flows trying to relax into a steady state. They do not represent the actual evolution of the physical system. Only the final picture for each set of parameters may coincide with experimentally realizable diode operation. It is those final steady-state pictures which comprise the core of the simulation results. One other thing to bear in mind is that in a physical diode, ion emission is not generally initiated simultaneously with electron emission. Rather, time integrated electron flow to the anode foil deposits either sufficient amounts of energy over the impact regions to cause vaporization

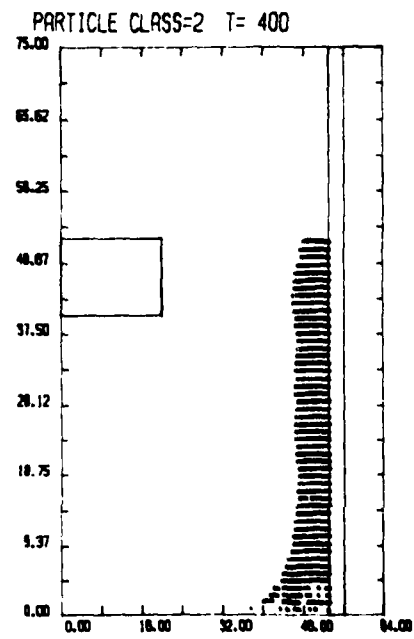
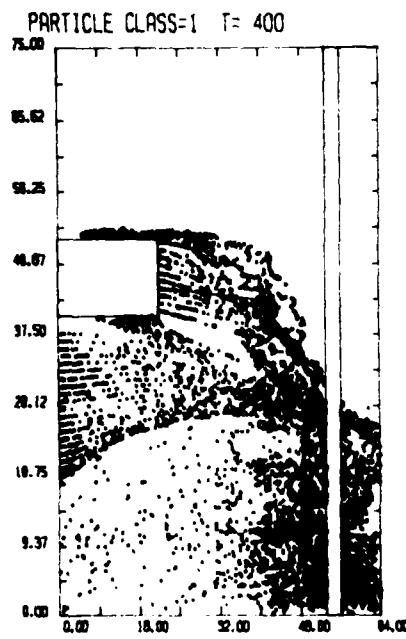
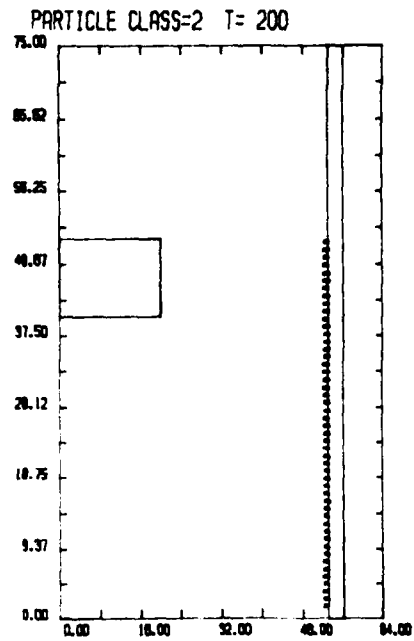
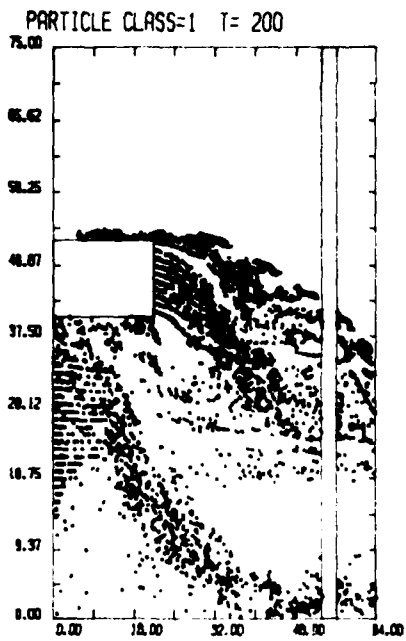


Fig. 8a - Early time evolution of the $I_w = 0$ case

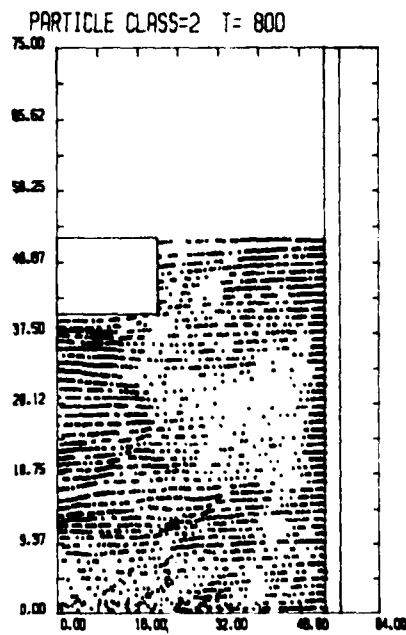
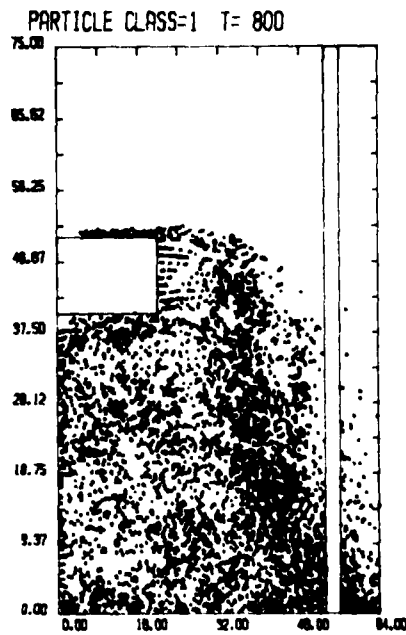
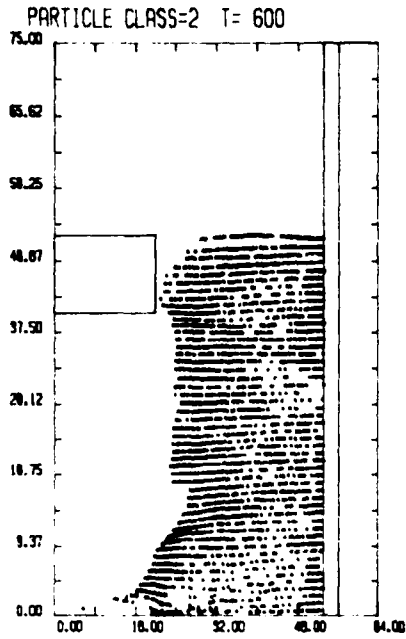
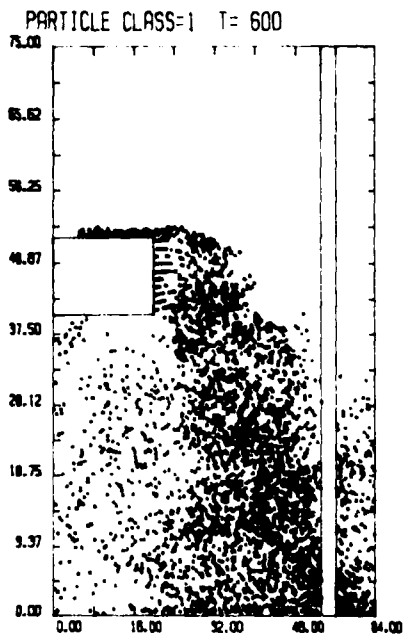


Fig. 8b - Late time evolution of the $I_w = 0$ case

and ionization or sufficient amounts of charge to cause surface flashover and ionization. In either case, the anode plasma thus formed acts as the source for protons in the diode.

Keeping in mind that only the equilibrium state will be "correct" it is nevertheless instructive to follow the sequence of events in Figure 8. At $T = 200 \Delta t$ the newly emitted ions have barely moved. The electron flow governed by its strong self-fields takes the form of two distinct streams. The numerical restriction of particle emission strictly to data cell centers allow for streamline tracing in all but the turbulent regions. In this far-from-steady condition, the electron current emitted is about 580 kiloamps, while that collected is a mere 240 kA. Emitted ion current is erratic, but appears to be around 150 kA. At $T=400 \Delta t$, the ions have advanced significantly with those at lower radii making up the vanguard due to the electric field enhanced by the focused electron charge near $R = 0$ at the anode. Attracted by the previously unneutralized ion space charge, the electron flow has unified into a single, neatly reflexing stream. (Note that in this run, the inner anode foil which forms the rightmost boundary of each frame is taken to be an electron-absorbing, solid conductor.) Notice that the regions or densest electron space charge at lower radii correspond to the space occupied by the advancing ion front. The net emitted and collected electron currents are 600 and 300 kiloamps, respectively, while ion emission has risen to about 350 kA. Turning to Figure 8b, $T= 600 \Delta t$ reveals the ion front racing along near its full velocity. It is just about to make contact with face of the cathode shank. Two important characteristics of the electron flow deserve mention: 1) this flow is strongly pinched toward the center of the anode without much apparent reflexing (very typical of high impedance diodes), and 2) most of the electron space-charge is concentrated in regions containing ion charge. At this time $(I_e)_{emit} = 600$ kA, $(I_e)_{coll} = 300$ kA, and $(I_i)_{emit} = 230$ kA. Finally, by $T = 800 \Delta t$, the near-equilibrium flow has set in. Electrons completely fill the inner diode cavity. The strongly pinched electron flow remains while the ion streams are fairly uniform. A word of caution -- the sparsely dotted area in the ion picture is an artifact of the non-random particle plotter; it does not translate to an actual absence of ions there. This configuration was allowed to continue for additional 200 timesteps. At that point (see Figure 9), the equilibrium currents were $I_e = 326$ kA and $I_i = 287$ kA. This total current of 613 kiloamps translated to an impedance of 6.5Ω which was too low for our desired operating regime.

In order to correct this, ion emission from the anode foil was "turned off" opposite the cathode shank. This could be accomplished experimentally by overlaying the anode foil with a metal foil there. Protons were then only injected from $R = 0$ out to the last cell just below the shank inner radius, $R = 4.0$ cm. The system evolved for another 1000 timesteps to the flow pattern depicted in Figure 10. Very little change from the electron flow of Figure 9 can be detected. At this stage, note that the inner anode foil is still taken to be a solid, electron-absorbing surface. The new quasi-static currents were $I_e = 264$ kA and $I_i = 214$ kA, yielding a net impedance of 8.4Ω for the diode. This was chosen as the reference steady-state against which the magnetic dam results are to be compared.

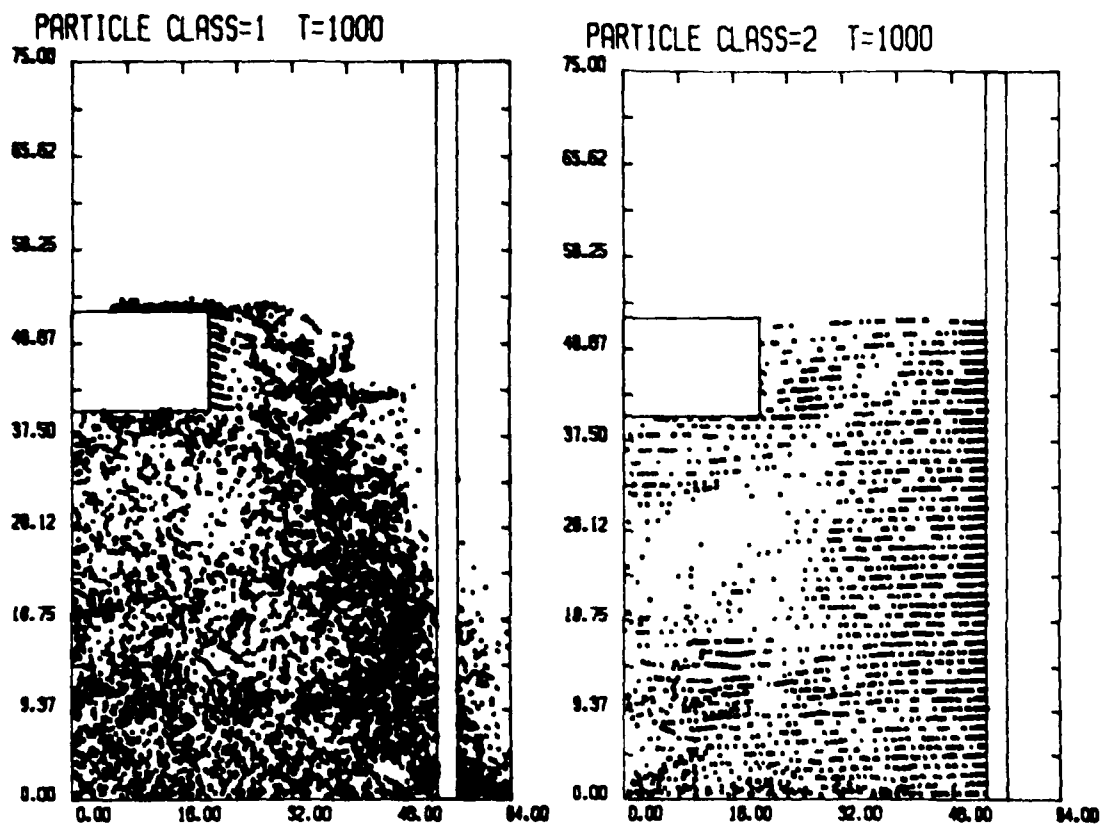


Fig. 9 - Steady-state particle positions for $I_w = 0$

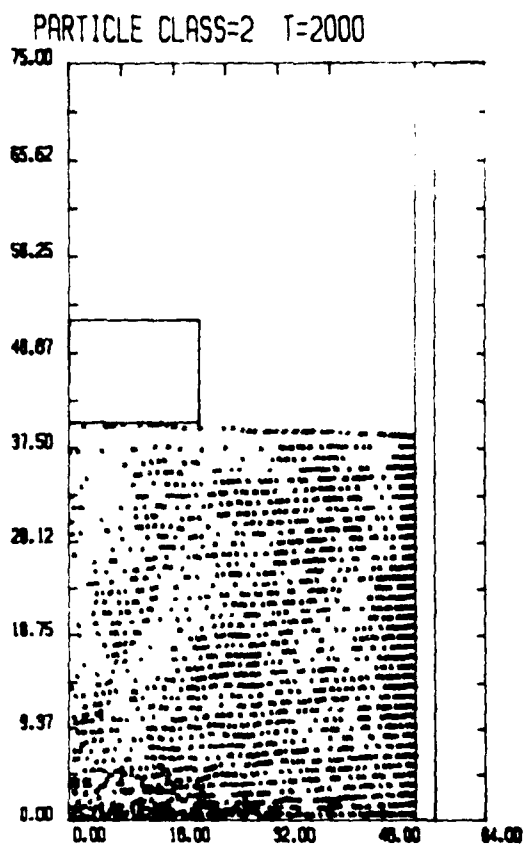
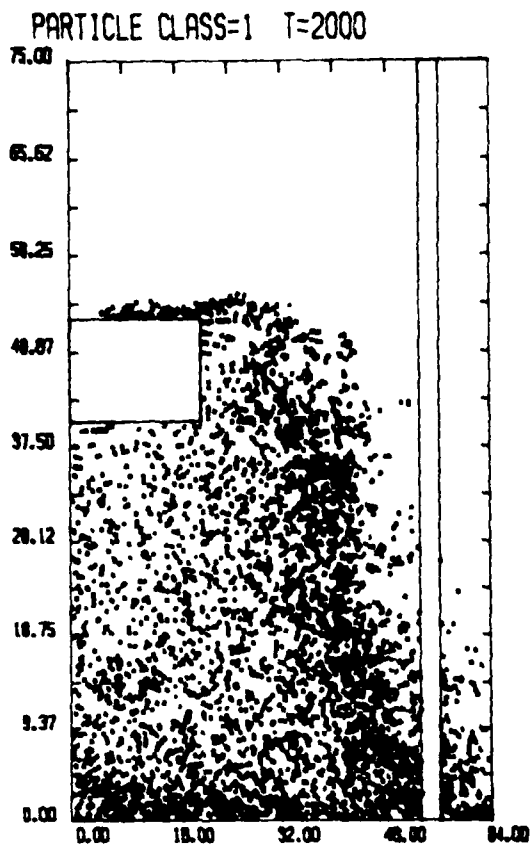


Fig. 10 — Steady-state particle positions for $I_w = 0$ with restricted ion emission

Retaining the same voltage, geometry and emission surfaces as those used for the 8.4 Ω reference case, the magnetic dam was then "turned on" by sending 65 kA through its central wire. The new particle positions for $T = 2400 \Delta t$ are shown in Figure 11. There are two things immediately apparent: first, the radial deflection of the electron flow due to the gas cell is unacceptably large as might have been predicted from Figures 3 and 4 and, second, an improved particle position plotter is required in which the z - range is extended into the "gas cell" so that the electrons there can be plotted. To remedy the first problem, I_w was doubled to 130 kiloamps. In order to alleviate the second, the axial width of the plotting page was increased from 64 ΔZ to 100 $\Delta Z = 3.0$ centimeters. Before moving on to this new case, it was recorded that the quasi-static currents were $I_e = 309$ kA and $I_i = 232.5$ kA. A true steady-state had not been reached, but it was decided not to invest additional funds to pursue such a non-promising run.

In addition to the doubling of I_w , the double anode foil configuration was eliminated for the remainder of the simulation runs. Referring back to Figure 1, the inner foil to which the wire was originally attached has now been completely removed. The quarter-centimeter vacuum gap is now treated numerically the same as the rest of the gas cell with the wire now running all the way to the outer anode foil. To accomplish this change in physical set-up required only the shifting of the electron "flag" setting boundary from $Z = 64 \Delta Z$ to $Z = 56 \Delta Z$ (See discussion at end of Section III). The original double-foil configuration probably contributed little to the magnetic dam physics but only served the practical experimental purpose of retaining a solid I_w current path for use after vaporization of the outer, proton-source anode foil.

As already stated, the first run using this new configuration was carried out for the case of $I_w = 130$ kiloamperes. Snapshots of the equilibrium electron and ion flows are shown in Figure 12. It appears that significant electron flow still extends beyond the right boundary, 1.32 centimeters from the anode foil. Referring back to Figure 4, this should not be surprising. Electron trajectories beginning at $R = 2.0$ cm at 45° extend almost 1.9 cm. into the gas cell. The even steeper angle injection suggested by the cathode-to-anode electron streaming should easily account for even wider ranging electrons at lower radii. One particularly disappointing aspect of the picture is the configuration of the electron charge density at the anode. An enhanced electron cloud can clearly be seen behind the anode foil, in the gas cell. Only a very thin electron layer appears in front of the foil where it is needed to enhance the ion emission. This observation is borne out in the equilibrium diode currents of $I_e = 330$ kA and $I_i = 244$ kA. The ion current increase is modest over the $I_w = 0$ case. Much more significant, however, is the even greater increase in the electron current. The net result has been a decrease in diode impedance of over one ohm while the ion production efficiency has actually dropped slightly. This is a crucial point which will be discussed later.

One obstacle that may be impeding the increase of ion efficiency is the wide disparity between the strengths of the oppositely directed B_θ fields on either side of the anode foil. These fields are proportional to the respective axial currents which, inside $R=5.0$ cm, are -574 kA on the left-hand side, and +130 kA on the right-hand side. Clearly, any electron

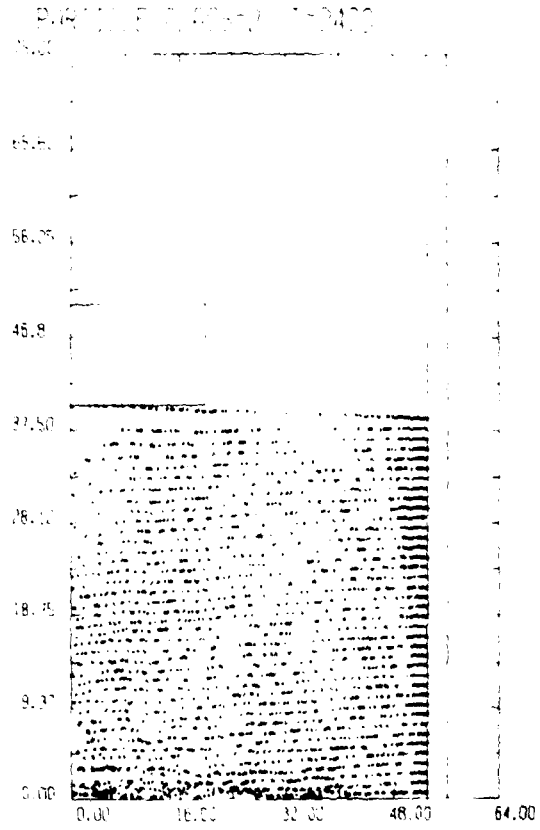
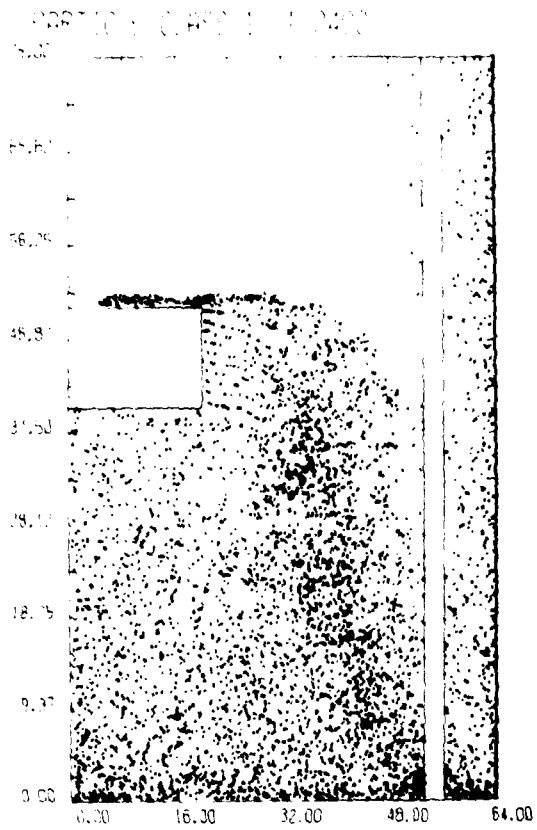


Fig. 11 — Quasi-equilibrium particle positions for $I_w = 65$ kA

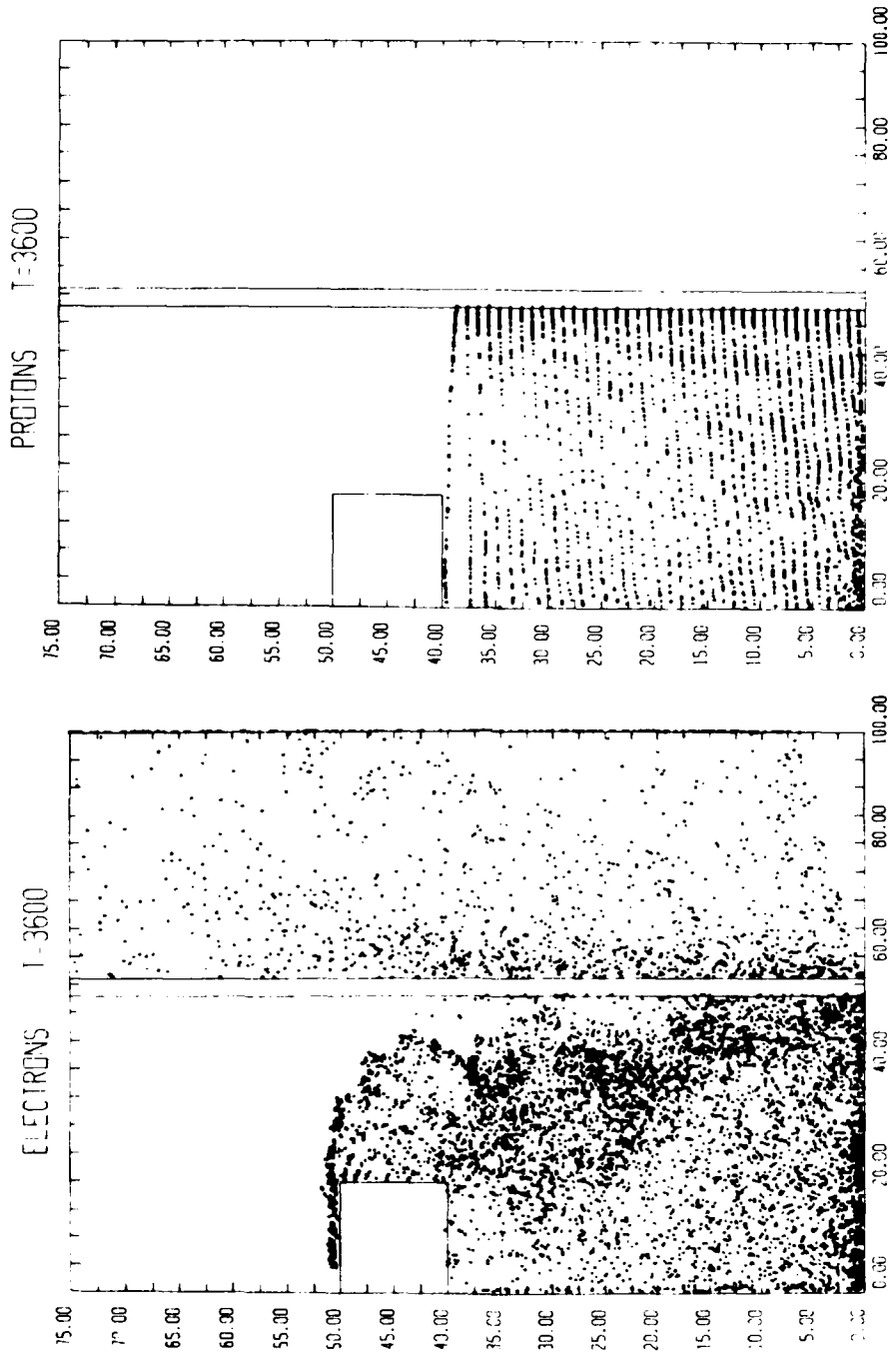


Fig. 12 — Steady-state particle positions for $I_w = 130$ kA

reflected back into the A-K gap will be quickly turned back into the gas cell. If "r" position will also be increased, resulting in a net outward radial electron flow. Thus, judging from the orbits of Figure 3 and 4, a typical electron might be bent back into the anode-cathode gap once below a radius of four centimeters. There, it will see a reverse B_0 approximately three times as great as that in the dam gas cell. After a gap drift time relatively short in comparison to that in the gas, the electron will be reflected back through the foil into a B_0 considerably weaker than that it had experienced in its previous trek through the gas. Thus, this "relative dwell time" problem snowballs with increasing radius as the gas B_0 decreases, while the gap B_0 increases. Reflected electrons spend progressively less a fraction of their time in the gap and progressively more in the gas at larger values of "r" where the larger electron gap dwell times would be felt over larger ion emission areas. In an attempt to redress this imbalance, a larger value of I_w was tested.

Although it would probably be somewhat difficult to accomplish experimentally, the current in the anode cell wire was boosted to 300 kA and the simulation was allowed to continue. A steady state was arrived at about $T = 4800 \Delta t$. The respective new flow patterns are presented in Figure 13. It would appear that an almost symmetric electron space-charge now hovers around the anode foil above about 1.5 centimeters radius. However, a large fraction of the electrons still penetrate a centimeter or more into the gas cell before reflection. This is in agreement with the predictions of Figure 4. The new currents are $I_e = 338 \text{ kA}$ and $I_i = 256.5 \text{ kA}$ yielding an even lower impedance and only slightly greater ion efficiency than those for the $I_w = 130 \text{ kA}$ case. The problem seems to be essentially the same as that for the previous case. An additional difficulty is suggested by the serious distortion of the main-stream shank electron flow away from the upper anode foil. This could easily cause degradation of the resultant ion emission.

All of these numerical results are summarized in Table 1. In this table, the term "ion production efficiency" is simply defined as I_{ion} / I_{diode} . Given the fixed voltage of the device, this ratio represents that fraction of the net diode power that has been imparted to the ions. The final two items in the tables are the total specie charges, Q , present in the diode/gas cell system. When these quantities have only small fluctuations during a simulation, one knows that the diode has reached an equilibrium state. Note the jump in Q_e when electrons are allowed to fill the gas cell for the $I_w = 65 \text{ kA}$ case. The steady reduction of Q_e in the subsequent two cases is indicative of the decreased volume accessible to the electrons in their more constrained excursions into the gas cell. Both I_i and Q_i steadily increase for increasing I_w , establishing the effectiveness of the dam at enhancing ion emission. The disappointing stagnation of the ion efficiency, combined with the consistent drop in diode impedance, however, indicates a proportional enhancement of electron emission.

The modest nature of the ion emission enhancement is obviated by Figure 14. For the higher values of I_w , otherwise significant gains in J_1 on some regions of the anode foil are offset by the strong suppression of emission in other regions. This suppression is probably due to the deflection of the main cathode-shank-to-anode electron stream away from certain areas of the anode foil face. Nevertheless, there is a net gain in ion current. Thus, the true

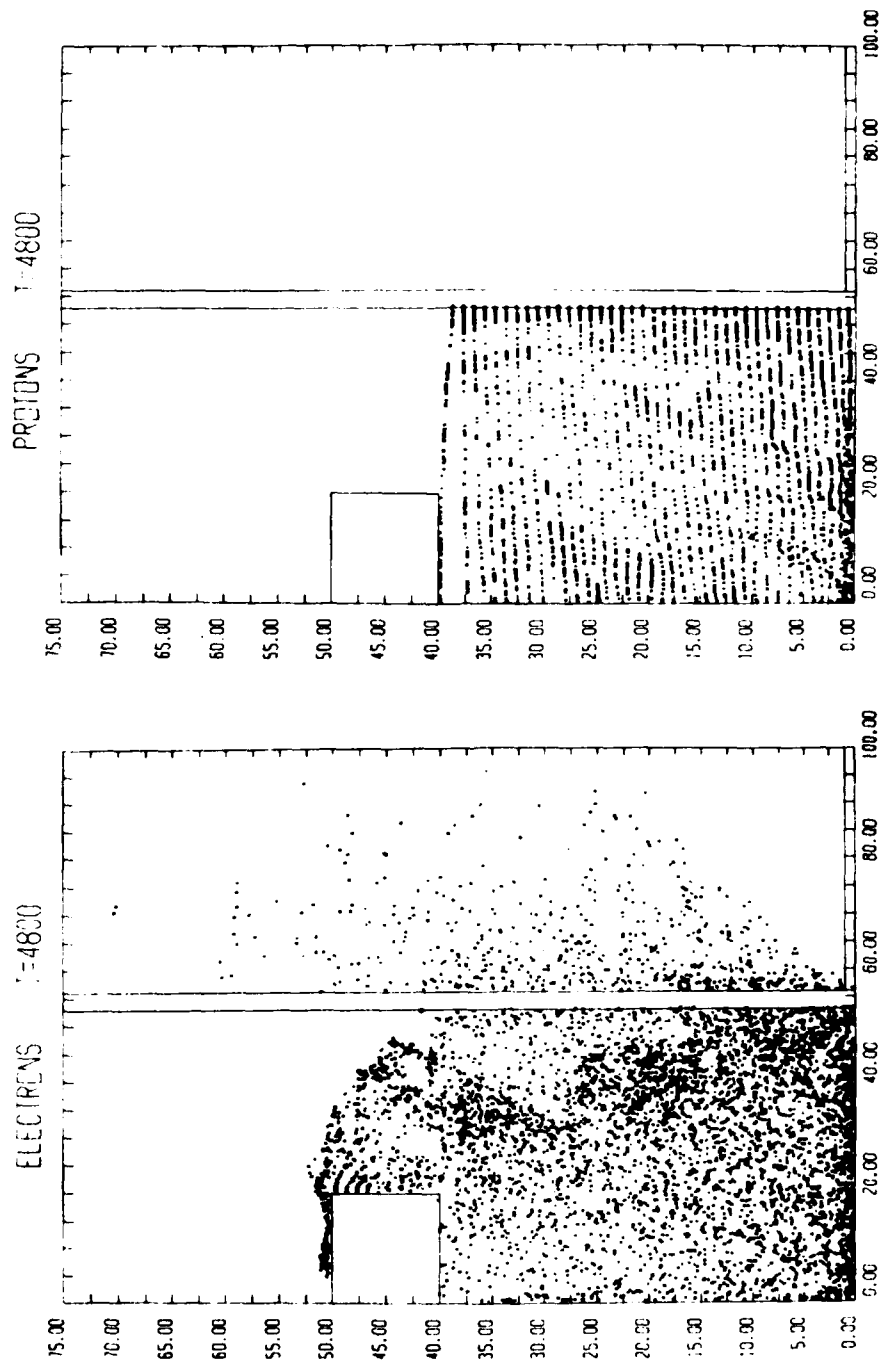


Fig. 13 — Steady-state particle positions for $I_w = 300$ kA

Table 1

I_{wire} (kA)	0	65	130	300
Simulation Timestep	2000	2400	3600	4800
I_{electron} (kA)	263.5	309	330	338
I_{ion} (kA)	214	232.5	244	256.5
I_{diode} (kA)	477.5	541.5	574	594.5
Ion Efficiency	0.448	0.429	0.425	0.431
Diode Impedance	8.4	7.4	7.0	6.7
Net Electron Charge (kilostatcoulombs)	-613	-898	-879	-782
Net Ion Charge (kilostatcoulombs)	+498	+539	+593	+615

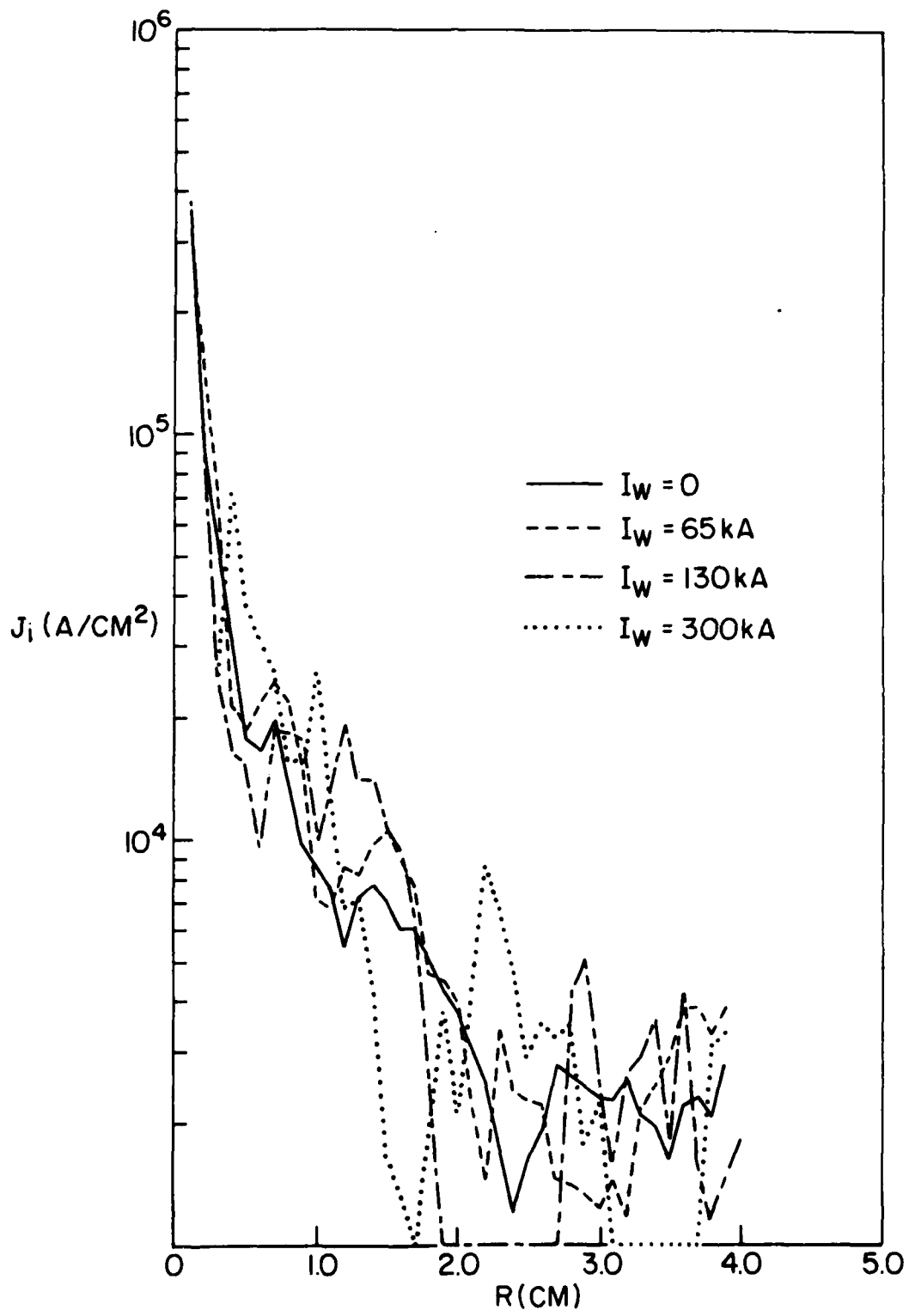


Fig. 14 - Emitted ion current density profiles along anode foil

obstacle to higher ion efficiency is the steady, net gain in electron current which results in a mild "bootstrapping"⁷ of the total diode current with increasing I_w .

Some insight into the cause of this phenomenon may be derived from a comparison of the respective equilibrium equipotential plots for each of the four cases. These are presented in Figure 15. The plot for $I_w = 65$ is something of an anomaly. This is understandable, since it has not yet reached a true steady state. The other three plots, however, show a definite migration of the potential contours toward the face of the cathode shank. This corresponds to an increased emission there. Electron emission also increased along the cathode foil for larger values of I_w . Interestingly enough, the inner and outer shank surfaces showed a decrease in emitted electron current, perhaps due to the stronger insulating B_0 fields which accompanied the larger net diode currents.

In order to propose more meaningful solutions, it is first necessary to more closely isolate the source of the excess I_e . For that purpose, the radial profiles of emitted electron current densities along the cathode shank face are plotted in Figure 16. Above 4.7 centimeters, the curves are virtually identical. On the lower half of the face, however the difference is marked. This agrees with the electric field enhancement there suggested in Figure 15. In fact, a full 75% of each increase is accounted for by the increase of I_e from the shank face. Specifically, $(I_e)_{total}$ increased 66.5 kA between the $I_w = 0$ and $I_w = 130$ kA cases; the shank face electron emission had increased by 49 kA. The total increase between $I_w = 130$ kA and $I_w = 300$ kA amounted to only 8kA of electron current; 6 kA of this difference can be attributed to the shank face. Simply stated, it appears that enhanced ion emission at higher radii increases the positive ion space charge in the A-K gap near the shank face sufficiently to enhance electron emission there. This, in turn, prohibited any increase in net ion production efficiency.

In conclusion, therefore, the dam diode pictured in Figure 1 does not appear to be effective in boosting ion efficiency in its present form. It does produce enhanced ion current but does not simultaneously reduce the diode electron current. A large part of the blame rests on the rapid outward radial migration of electrons along the anode foil and on the large disparity between typical electron lifetimes in the gas cell versus those in the gap. This limits the number of electrons available in the upper A-K gap to neutralize the positive space charge arising there due to the increased ion flow. Hence electric fields and electron emission along the lower face of the cathode shank are made larger.

A modification which could possibly rectify this situation would be to invert the radial dependence of the magnetic field strength in the anode gas cell. If it were directly rather than inversely proportional to radius, then electron gyroradii would progressively decrease as they moved outward, increasing the "dwell time" of electron space charge in the crucial region between $R = 3.0$ and $R = 5.0$ centimeters. That would accomplish both an enhancement of ion emission over relatively large surface areas of the anode foil and also a probable suppression of electron emission along the cathode shank face located only one centimeter away. A possible alternative, and one easier to realize experimentally, is to absorb all electrons hitting the anode

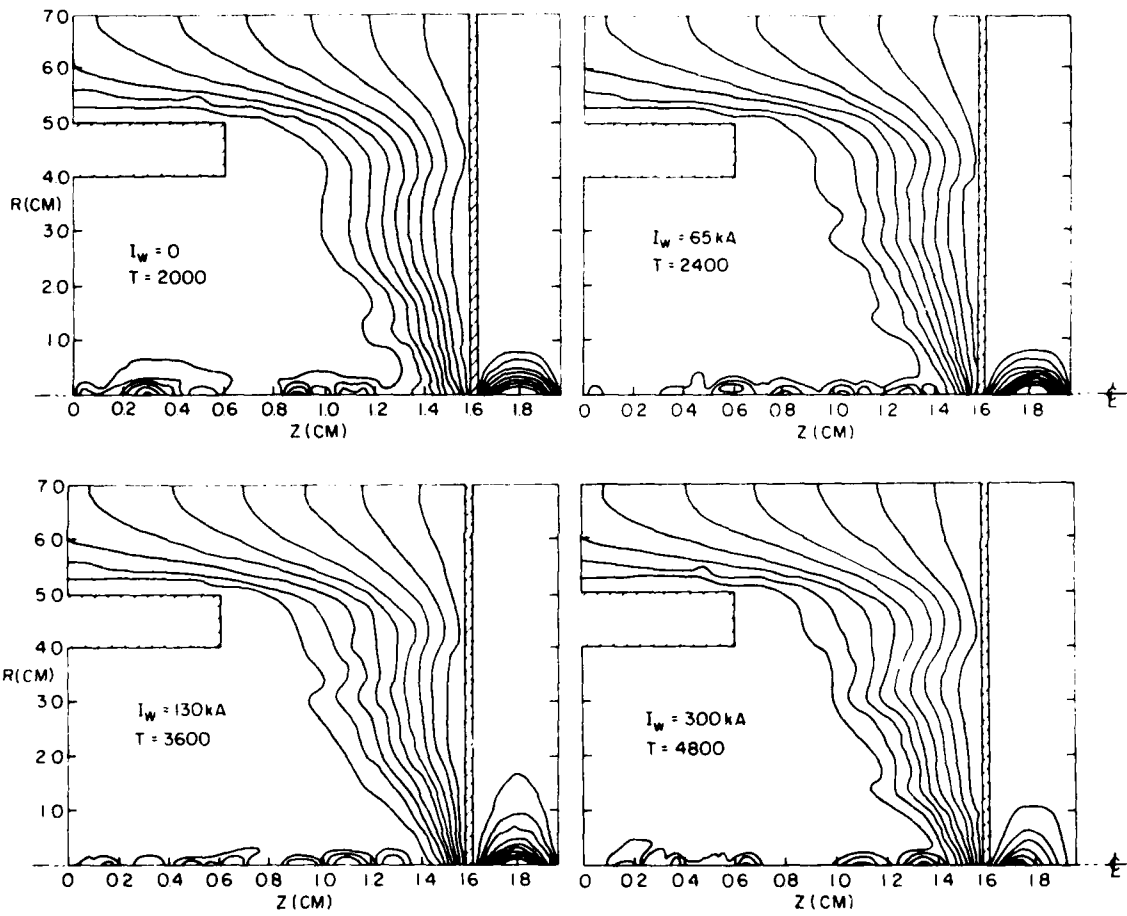


Fig. 15 — Steady-state equipotential contours for the four cases

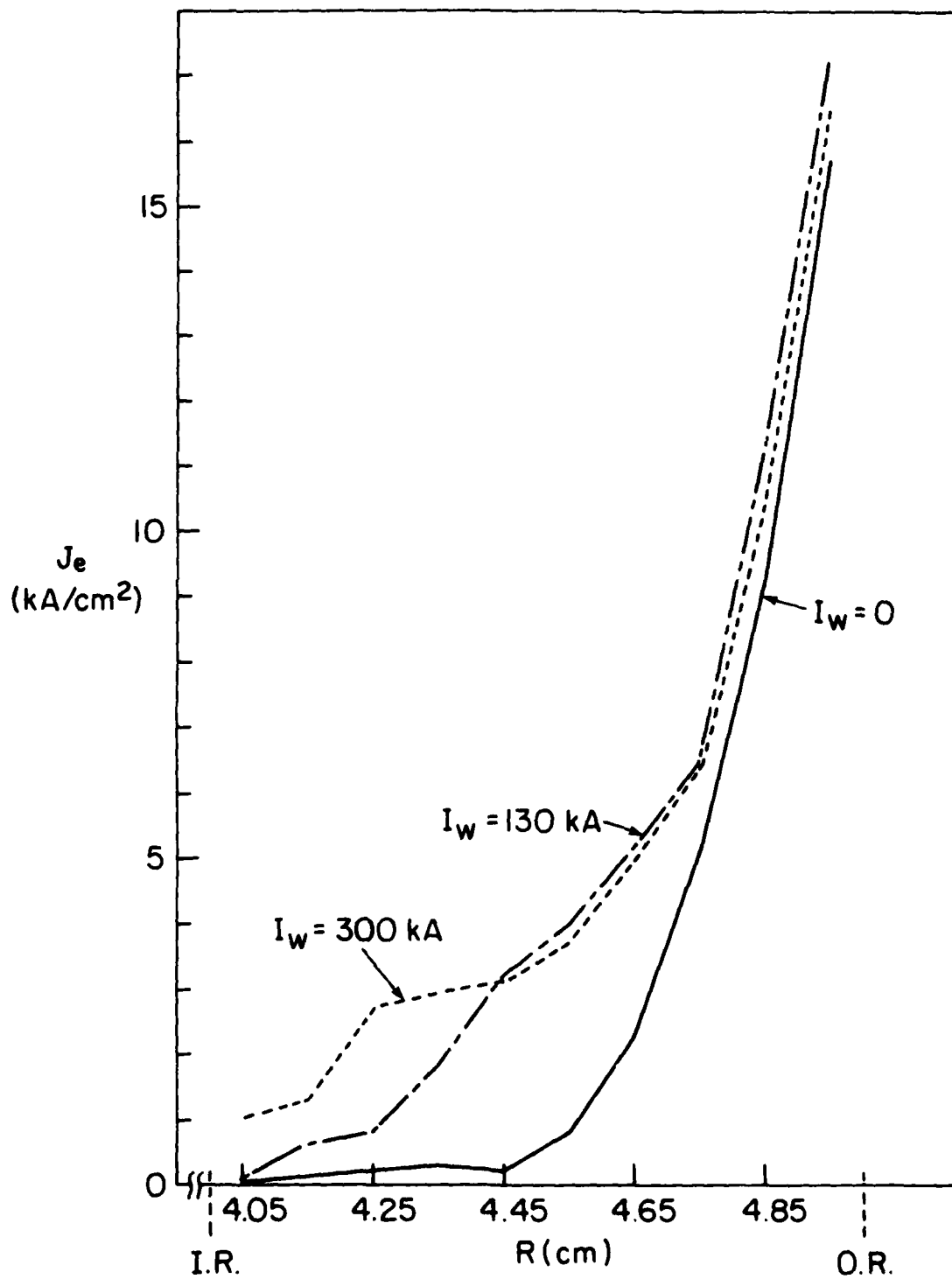


Fig. 16 - Radial profiles of electron emission along face of cathode shank

foil above, say, 3.0 centimeters while leaving the dam field inversely proportional to radius. This reduces the electron space charge near the anode foil above $r=3$, reducing the ion emission above $r=3$, reducing ion space charge in the gap above $r=3$, reducing electric field strengths at the cathode shank face, reducing electron emission there. This mandates an increase of this diode's impedance for a fixed gap and voltage. Both of the above modifications will be simulated in future computational experiments to test their ability to boost the ion production efficiency.

REFERENCES

1. S. J. Stephanakis, D. Mosher, Shyke A. Goldstein, W. F. Oliphant, Roswell Lee, and G. Cooperstein, *Bull. Am. Phys. Soc.* 22, 1130 (1977).
2. S. J. Stephanakis, J. R. Boller, G. Cooperstein, Shyke A. Goldstein, D. D. Hinshelwood, D. Mosher, W. F. Oliphant, F. Sandel, and F. C. Young, *Bull. Am. Phys. Soc.* 23, 907 (1978).
3. S. J. Stephanakis, J. R. Boller, G. Cooperstein, Shyke A. Goldstein, D. D. Hinshelwood, D. Mosher, W. F. Oliphant, F. C. Young, R. D. Genuario, and J. E. Maenchen, *Bull. Am. Phys. Soc.* 24, 1031 (1979).
4. S. A. Goldstein and P. F. Ottinger, JAYCOR Report No. TPD200-80-003-FR, (1980).
5. R. J. Barker, A. T. Drobot, Roswell Lee, and S. A. Goldstein, Proc. 9th Conference on the Numerical Simulation of Plasmas, Evanston, Ill. (1980).
6. R. J. Barker, *Banach Center Publications* 3, 255, Warsaw, Poland (1975).
7. R. J. Barker, S. A. Goldstein, and R. E. Lee, *IEEE Int. Conf. on Plasma Science*, Montreal, Canada (1979).

DISTRIBUTION LIST

Director Defense Intelligence Agency Washington, DC 20301		Commander Harry Diamond Laboratories 2800 Powder Mill Road Adelphi, MD 20793 (CNWDI-INNER ENVELOPE: ATTN: DELHD-RBH)	
Attn: DTICI Robert I. Rubenstein	1 copy		
Defense Advanced Research Project Agency 1400 Wilson Blvd. Arlington, VA 22209 Attn: J. Bayless	1 copy	Attn: DELHD-NP DELHD-RCC J. A. Rosado DRXDO-RBH P. A. Caldwell DRXDO-RBH D. Schallhorn DRXDO-PI Tech Lib. S. Graybill	1 copy 1 copy 1 copy 1 copy 1 copy 1 copy
Director Defense Nuclear Agency Washington, DC 20305		Commander Picatinny Arsenal Dover, NJ 07801	
Attn: FCPR STVL TISI Archives TITL Tech. Library J. Z. Farber (RAEV) R. L. Gullickson (RAEV)	1 copy 1 copy 1 copy 3 copies 1 copy 1 copy	Attn: SMUPA ND-N-E	1 copy
Defense Technical Information Center Cameron Station 5010 Duke Street Alexandria, VA 22314		U. S. Air Force Office of Scientific Research Physics Directorate Bolling A.F.B., DC 20332	
Attn: T. C.	12 copies	Attn: A. K. Hyder M. A. Stroschio	1 copy 1 copy
Under Sec'y of Defense for RSCH and ENGRG Department of Defense Washington, DC 20301		Commander U. S. Army Missile Command Redstone Arsenal, AK 35809	
Attn: S&SS(OS)	1 copy	Attn: Redstone Scientific Information CTR DRCPM-PM-PE-EA	1 copy
Chief Livermore Division Fld Command DNA Lawrence National Laboratory P. O. Box 808 Livermore, CA 94550		Commander U. S. Army Nuclear Agency 7500 Backlick Road Building 2073 Springfield, VA 22150	
Attn: FCPRL	1 copy	Attn: ATCN-w	1 copy
National Technical Information Service U.S. Department of Commerce 5285 Port Royal Road Springfield, VA 22161	24 copies	Commander U. S. Army Test and Evaluation COMD Aberdeen Proving Ground, MD 21005	
Commander BMD System Command P. O. Box 1500 Huntsville, AL 35807		Attn: DRSTi-EL	1 copy
Attn: SSC-TEN	1 copy	Commander Naval Electronic Systems CMD HQS Washington, DC 20360	
DEP Chief of Staff for RSCH DEV & ACQ Department of the Army Washington, DC 20310		Attn: Code 6032	1 copy
Attn: DAMA-CSM-N	1 copy	Commanding Officer Naval Intelligence Support Center 4301 Suitland Road - Building 5 Washington, DC 20390	
		Attn: NISC-45	1 copy

Naval Research Laboratory		SAMSO/DY	
Addressee: Attn: Name/Code		Post Office Box 92960	
Code 2628 - TIC-Distribution	25 copies	Worldway Postal Center	
Code 4020 - J. Boris	1 copy	Los Angeles, CA 90009	
Code 6682 - D. Nagel	1 copy	(Technology)	
Code 4700 - T. Coffey	26 copies	Attn: DYS	1 copy
Code 4707 - J. Davis	1 copy		
Code 4730 - S. Bodner	1 copy	SAMSO/IN	
Code 4740 - V. Granatstein	1 copy	Post Office Box 92960	
Code 4760 - B. Robson	1 copy	Worldway Postal Center	
Code 4761 - C. Kapetanakis	1 copy	Los Angeles, CA 90009	
Code 4770 - Branch Head	10 copies	Attn: IND MAJ D. S. Muskin	1 copy
Code 4770 - F. Young	1 copy		
Code 4770 - S. Stephanakis	1 copy		
Code 4771 - D. Mosher	10 copies		
Code 4773 - G. Cooperstein	10 copies		
Code 4790 - D. Colombant	1 copy		
Code 4790 - I. Haber	1 copy	SAMSO/MN	
Code 4790 - M. Lampe	1 copy	Norton AFB, CA 92409	
On-Site Contractors:		(Minuteman)	
Code 4770 - R. Barker (Jaycor)	1 copy	Attn: MNNH	1 copy
Code 4770 - S. Goldstein (Jaycor)	1 copy		
Code 4770 - R. Meger (Jaycor)	1 copy		
Code 4770 - P. Ottinger (Jaycor)	1 copy		
Code 4770 - F. Sandel (Jaycor)	1 copy		
Code 4790 - A. Drobot (SAI)	1 copy		
		SAMSO/SK	
Officer-in-Charge		Post Office Box 92960	
Naval Surface Weapons Center		Worldway Postal Center	
White Oak, Silver Spring, MD 20910		Los Angeles, CA 90009	
		(Space Comm Systems)	
Attn: Code WR43	1 copy	Attn: SKF P. H. Stadler	1 copy
Code WA501 - Navy Nuc Prgms Off	1 copy		
		U. S. Department of Energy	
Chief of Naval Operations		Division of Inertial Fusion	
Navy Department		Washington, DC 20545	
Washington, DC 20350		Attn: G. Canavan	1 copy
Attn: R. A. Blaise 604C4	1 copy	T. F. Godlove	1 copy
		S. L. Kahalas	1 copy
		R. L. Schriever	1 copy
Commander		Argonne National Laboratory	
Naval Weapons Center		9700 South Cass Avenue	
China Lake, CA 93555		Argonne, Illinois 60439	
Attn: Code 533 Tech Lib.	1 copy	Attn: G. R. Magelssen	1 copy
		R. J. Martin	1 copy
AF Weapons Laboratory, AFSC		Brookhaven National Laboratory	
Kirtland AFB, NM 87117		Upton, NY 11973	
Attn: CA	1 copy	Attn: A. F. Maschke	1 copy
ELC	1 copy		
NT	1 copy	Lawrence Berkley Laboratory	
SUL	1 copy	Berkeley, CA 94720	
DYP	1 copy	Attn: D. Keefe	1 copy
J. Darrah	1 copy		
W.L. Baker	1 copy		
HQ USAF/RD		Lawrence Livermore National Laboratory	
Washington, DC 20330		P. O. Box 808	
Attn: RDQSM	1 copy	Livermore, CA 94550	
		Attn: L-18	1 copy
Director		L-153	1 copy
Joint Strat TGT Planning Staff JCS		R. O. Bangerter	1 copy
OFFUTT AFB		R. J. Briggs	1 copy
Omaha, NB 68113		E. P. Lee	1 copy
Attn: JSAS	1 copy	J. H. Nuckolls	1 copy
		S. S. Yu	1 copy
		Tech Info Dept. L-3	1 copy

Los Alamos National Laboratory
P. O. Box 1663
Los Alamos, NM 87545

Attn: D. B. Henderson
R. B. Perkins
L. E. Thode

1 copy
1 copy
1 copy

National Science Foundation
Mail Stop 19
Washington, DC 20550

Attn: D. Berley

1 copy

Sandia National Laboratories
P. O. Box 5800
Albuquerque, NM 87185

Attn: J. R. Freeman / 4241
S. Humphries / 4253
D. J. Jonnson / 4244
G. W. Kuswa / 4240
P. A. Miller / 4244
J. P. Vandevender / 4252
G. Yonas / 4200
Doc Con for 3141 Sandia RPT Coll

1 copy
1 copy

AVCO Research and Systems Group
201 Lowell Street
Wilmington, MA 01887

Attn: Research Lib. A830 Rm. 7201

1 copy

BDM Corporation, The
795 Jones Branch Drive
McLean, VA 22101

Attn: Tech Lib.

1 copy

Bechtel Group, Inc.
P.O. Box 3965
San Francisco, CA 94119

Attn: W. O. Allen

1 copy

Boeing Company, The
P. O. Box 3707
Seattle, WA 98124

Attn: Aerospace Library

1 copy

Cornell University
Ithaca, NY 14850

Attn: D. A. Hammer
R. N. Sudan
J. Maenchen

1 copy
1 copy
1 copy

The Dikewood Corporation
1613 University Blvd., NE
Albuquerque, NM 87102

Attn: L. Wayne Davis

1 copy

EG&G, Inc.
Albuquerque Division
P. O. Box 10218
Albuquerque, NM 87114

Attn: Technical Library

1 copy

Ford Aerospace & Communications Operations
Ford & Jamboree Roads
Newport Beach, CA 92663
(Formerly Aeronutronic Ford Corporation)

Attn: Tech Info Section

1 copy

General Electric Company
Space Division
Valley Forge Space Center
Goddard Blvd., King of Prussia
P. O. Box 8555
Philadelphia, PA 19101

Attn: J. C. Penden VFSC, Rm. 4230M

1 copy

General Electric Company
Tempo-Center for Advanced Studies
816 State Street (P. O. Drawer QQ)
Santa Barbara, CA 93102

Attn: DASIAC

1 copy

Grumman Aerospace Corporation
Bethpage, NY 11714

Attn: P. Suh

1 copy

Institute for Defense Analyses
400 Army-Navy Drive
Arlington, VA 22202

Attn: IDA Librarian R. S. Smith

1 copy

Ion Physics Corporation
South Beford Street
Burlington, MA 01803

Attn: H. Milde

1 copy

IRT Corporation
P. O. Box 91087
San Diego, CA 92138

Attn: R. L. Mertz

1 copy

JAYCOR, Inc.
205 S. Whiting Street
Alexandria, VA 22304

Attn: E. Alcaraz
J. Guillory
R. Hubbard
R. Sullivan
D. A. Tidman

1 copy
1 copy
1 copy
1 copy
1 copy

JAYCOR, Inc.
11011 Torreyana Road
San Diego, CA 92121

Attn: E. Wenaas

1 copy

Kaman Science Corporation
P. O. Box 7463
Colorado Springs, CO 80933

Attn: A. P. Bridges
D. H. Bryce
J. R. Hoffman
W. E. Ware

1 copy
1 copy
1 copy
1 copy

Lockheed Missiles and Space Co., Inc.
3251 Manover Street
Palo Alto, CA 94304

Attn: L. F. Chase

1 copy

Massachusetts Institute of Technology
Cambridge, MA. 02139

Attn: R.C. Davidson
G. Bekefi
D. Hinshelwood

1 copy
1 copy
1 copy

Maxwell Laboratories, Inc.
9244 Balboa Avenue
San Diego, CA 92123

Attn: R. W. Clark
A. C. Kolb
P. Korn
A. R. Miller
J. Pearlman

1 copy
1 copy
1 copy
1 copy
1 copy

McDonnell Douglas Corporation
5301 Bolsa Avenue
Huntington Beach, CA 92647

Attn: S. Schneider

1 copy

Mission Research Corporation
1400 San Mateo Blvd. SE
Albuquerque, NM 87108

Attn: B. B. Godfrey

1 copy

Mission Research Corporation-San Diego
P. O. Box 1209
LaJolla, CA 92038

Attn: V.A.J. Van Lint

1 copy

Mission Research Corporation
735 State Street
Santa Barbara, CA 93101

Attn: W. C. Hart
C. L. Longmire

1 copy
1 copy

Northrop Corporation
Electronic Division
2301 West 120th Street
Hawthorne, CA 90250

Attn: V. R. DeMartino

1 copy

Northrop Corporation
Northrop Research and Technology Ctr.
3401 West Broadway
Hawthorne, CA 90205

1 copy

Physical Dynamics
P.O. Box 556
La Jolla, CA 92037

Attn: S. Jorna

1 copy

Physics International Co.
2700 Merced Street
San Leandro, CA 94577

Attn: J. Benford
B. Bernstein
G. Frazier
R. Genuario
E. B. Goldman
R. Huff
A. J. Toepfer

1 copy
1 copy
1 copy
1 copy
1 copy
1 copy
1 copy

Pulsar Associates, Inc.
11491 Sorrento Valley Blvd.
San Deigo, CA 92121

Attn: C. H. Jones, Jr.

1 copy

Princeton Plasma Physics Laboratory
James Forrestal Campus
P.O. Box 451
Princeton, N.J. 08540

Attn: R. Kulsrud

1 copy

Pulse Sciences, Inc.
1615 Broadway, Suite 610
Oakland, CA 94612

Attn: I. Smith
P. Spence
S. Putman

1 copy
1 copy
1 copy

R&D Associates
P. O. Box 9695
Marina Del Rey, CA 90291

Attn: W. R. Graham, Jr.
M. Grover
C. MacDonald
E. Martinelli

1 copy
1 copy
1 copy
1 copy

R&D Associates
Suite 500
1401 Wilson Blvd.
Arlington, VA 22209

Attn: P. J. Turchi

1 copy

Science Applications, Inc.
P. O. Box 2351
LaJolla, CA 92038

Attn: J. Robert Beyster

1 copy

Spire Corporation P. O. Box 9 Bedford, MA 01730		University of Rochester Laboratory of Laser Energetics River Station, Hopeman 110 Rochester, NY 14627	
Attn: R. G. Little	1 copy	Attn: M. J. Lubin	1 copy
SRI International 333 Ravenswood Avenue Menlo Park, CA 94025		University of Scranton Dept. of Physics Scranton, PA 18510	
Attn: Setsuo Odairiki	1 copy	Attn: F. Murray	1 copy
Stanford University SLAC P. O. Box 4349 Stanford, CA 94305		U. S. Department of Energy P. O. Box 62 Oak Ridge, TN 37830	50 copies
Attn: W. B. Herrmannsfeldt	1 copy	Vought Corporation Michigan Division 38111 Van Dyke Road Sterling Heights, MI 48077 (Formerly LTV Aerospace Corp)	
Systems, Science and Software, Inc. P. O. Box 1620 LaJolla, CA 92038		Attn: Tech Lib	1 copy
Attn: A. R. Wilson	1 copy	Atomic Weapons Research Establishment Building H36 Aldermaston, Reading RG 7 4PR United Kingdom	
Texas Tech University P. O. Box 5404 North College Station Lubbock, TX 79417		Attn: J. C. Martin	1 copy
Attn: T. L. Simpson	1 copy	Bhabha Atomic Research Centre Bombay - 400085, India	
TRW Defense and Space Sys Group One Space Park Redondo Beach, CA 90278		Attn: B. K. Godwal A. S. Paithankar	1 copy 1 copy
Attn: Tech Info Center/S-1930 Z.G.T. Guiragossian D. Arnush	1 copy 1 copy 1 copy	CEA, Centre de Etudes de Lemeil B. P. 27 94190 Villeneuve, Saint George France	
University of California Dept. of Physics La Jolla, CA 92037		Attn: A. Bernard A. Jolas	1 copy 1 copy
Attn: K. Brueckner W.B. Thompson	1 copy 1 copy	CEA, Centre de Etudes de Valduc P. B. 14 21120 Is-sur-Tille France	
University of California Boelter Hall 7731 Los Angeles, CA 90024		Attn: J. Barbaro C. Bruno N. Camarcot C. Patou C. Peugeot	1 copy 1 copy 1 copy 1 copy 1 copy
Attn: F.F. Chen	1 copy	Centro Di Frascati C.P.N. 65 00044 Frascati (Roma) Italy	
University of California Irvine, CA 90024		Attn: J.P. Rajer	1 copy
Attn: G. Benford N. Rostoker	1 copy 1 copy		
University of Illinois Urbana, IL 61801			
Attn: G. H. Miley J. T. Verdeyen	1 copy 1 copy		

Culham Laboratories UKAEA Ebingdon, Birks. England		Institute of Nuclear Energy Research Atomic Energy Council P.O. Box 3 - Lung-Tan, Taiwan Republic of China	
Attn: N. J. Peacock	1 copy	Attn: C. Chang	1 copy
Ecole Polytechnique Labo. PMI 91128 Palaseau Cedex France		Instituto De Investigaciones Cientificas Y Technicas De Las Fuerzas Armadas Aufriategui y Varela V. Martelli 1603 Pcia Bs. As. - R. Argentina	
Attn: J. M. Buzzi H. Doucet	1 copy 1 copy	Attn: N. B. Camusso	1 copy
Ecole Polytechnique Labo. PMI 91128 Palaseau Cedex France		Max-Planck-Institut fur Plasmaphysik 8046 Garching bei Munchen West Germany	
Attn: J.M. Buzzi H. Doucet	1 copy 1 copy	Attn: R. Lengyel I. Hofmann	1 copy 1 copy
Institut d'Electronique Fondamentale Universite' Paris XI-Bat. 220 F91405 Orsay France		Physical Research Laboratory Navrangpura Ahmedabad - 380009 - India	
Attn: G. Gautherin	1 copy	Attn: V. Ramani P. I. John	1 copy 1 copy
Institut fur Angewandte Physik Robert Mayer Str. 2-4 D6000 Frankfurt, West Germany		Shivaji University Kolhapur, India	
Attn: H. Deitinghoff H. Klein	1 copy 1 copy	Attn: L. N. Katkan	1 copy
Institut Fur Neutronenphysik un Reaktortechnik Postfach 3640 Kernforschungszentrum D-7500 Karlsruhe 1 west Germany		Tokyo Institute of Technology The Graduate School at Nagatsuta 4259 Nagatsuta, Midori-Ku Yokohama 227, Japan	
Attn: H. Bluhm H. U. Karow W. Schmidt K.W. Zieher	1 copy 1 copy 1 copy 1 copy	Attn: K. Niu S. Yamaguchi	1 copy 1 copy
Institute of Atomic Energy Academia Sinica P.O. Box 2125 Beijing People's Republic of China		Weizmann Institute of Science Rehovot, Israel	
Attn: W. Ganchang, Director R. Hong	2 copies 1 copy	Attn: A. E. Blaugrund E. Nardi Z. Zinamon	1 copy 1 copy 1 copy
Institute of Laser Engineering Osaka University Yamadakami Suita Osaka 565, Japan		Near Kanchan Bhawan Var Ruchi Marg, Madhav Nagar, Ujjain, (M.P.) INDIA	
Attn: K. Imasaki S. Nakai	1 copy 1 copy	Attn: Dr. R. K. Chhajlani	1 copy

JAYCOR, Inc.
11011 Torreyana Road
San Diego, CA 92121

Attn: S. S. Wang 1 copy

Los Alamos National Laboratory
P. O. Box 1663
Los Alamos, NM 87545

Attn: C. Barnes 1 copy

Mission Research Corporation
Capitol Building II, Suite 201
5503 Cherokee Avenue
Alexandria, VA 22312

Attn: B. Goplen 1 copy

Sandia National Laboratories
P. O. Box 5800
Albuquerque, NM 87185

Attn: J. Quintens/4252 1 copy

SRI International
333 Ravenswood Avenue
Menlo Park, CA 94025

Attn: R. J. Vidmar 1 copy

Stanford University
Dept. of Electrical Engineering
Stanford, CA 94305

Attn: O. Buneman 1 copy

Stanford University
Dept. of Mechanical Engineering
Stanford, CA 94305

Attn: M. Mitchner 1 copy
S. A. Self 1 copy

Stanford University
Hoover Institution
Stanford, CA 94305

Attn: D. L. Bark 1 copy

Stevens Institute of Technology
Dept of Physics
Castle Point Station
Hoboken, NJ 07030

Attn: W. Bostick 1 copy
V. Nardi 1 copy

Texas Tech University
P. O. Box 5404 - North College Station
Lubbock, TX 79417

Attn: M. Kristiansen 1 copy

US Air Force Academy
Dept. of Physics
Colorado, 80340

Attn: J. T. May 1 copy
D. Murawinski 1 copy

LMED
-8